T2R2 東京工業大学リサーチリポジトリ
Tokyo Tech Research Repository

論文 / 著書情報
Article / Book Information

題目(和文)	
Title(English)	Development of HER2-targeting small proteins by immobilization of binding-peptides in scaffold proteins
著者(和文)	YIMCHUENWANAPORN
Author(English)	Wanaporn Yimchuen
出典(和文)	学位:博士(工学), 学位授与機関:東京工業大学, 報告番号:甲第11559号, 授与年月日:2020年6月30日, 学位の種別:課程博士, 審査員:門之園 哲哉,近藤 科江,丸山 厚,小倉 俊一郎,堤 浩
Citation(English)	Degree:Doctor (Engineering), Conferring organization: Tokyo Institute of Technology, Report number:甲第11559号, Conferred date:2020/6/30, Degree Type:Course doctor, Examiner:,,,,
学位種別(和文)	博士論文
Type(English)	Doctoral Thesis

Powered by T2R2 (Tokyo Institute Research Repository)

東京工業大学
Tokyo Institute of Technology

Doctoral Dissertation

Academic Year 2020

Development of HER2-targeting small proteins by immobilization of binding-peptides in scaffold proteins

by

Wanaporn Yimchuen

School of Life Science and Technology

Department of Life Science and Technology

Academic advisor (main): Asst. Prof. Tetsuya Kadonosono

Academic advisor (sub): Prof. Shinae Kizaka-Kondoh

Table of Contents

Abbreviation Lists

Ab	Antibody
AbP	mAb-derived peptide
ADC	Antibody-drug conjugate
ADCC	Antibody-dependent cellular cytotoxicity
BLI	Bioluminescence imaging
CDC	Complement-dependent cytotoxicity
CDR	Complementarity determining regions
CSA	Constrained and solvent accessible
EGFR	Epidermal growth factor receptor
ELISA	Enzyme-linked immunosorbent assay
Fabs	Antigen-binding fragments of antibody
FDA	Food and Drug Administration
FLAP	Fluctuation-regulated affinity protein
FN3	Human tenth fibronectin type III domain
FR	Framework region
GA	Grafting acceptor
GST	glutathione-S-transferase
HBP	HER2-binding peptide
HBP-FLAP	HER2-binding fluctuation-regulated affinity protein
HER2	Human epidermal growth factor receptor-2
HPLC	High-performance liquid chromatography
Ig	Immunoglobulin
IHC	Immunohistochemistry
K_D	Dissociation constant

k_{on}	Association rate
k_{off}	Dissociation rate
mAb	Monoclonal antibody
MAPK	Mitogen-activated protein kinase
MD	Molecular dynamics
MW	Molecular weight
PDB	Protein Data Bank
p.i.	Post-injection
PI3K	Phosphatidylinositol-4,5-bisphosphate 3-kinase
RLuc	*Renilla* luciferase 8.6-535
RMSD	Root-mean-square deviation
RMSF	Root-mean-square fluctuation
SA	Solvent accessible
SASA	Solvent accessible surface area
scFv	Single chain Fv
SEM	Standard error of the mean
t1/2	Half-life
T/B	Tumor versus background
TK	Tyrosine kinases
T_m	Melt transition temperature

Chapter 1

General Introduction

1-1. Antibody for cancer research and therapy

Monoclonal antibodies (mAbs) have been utilized as one of the most successful strategies for cancer therapy because they selectively target cell surface antigens or marker proteins.[1] However, mouse mAbs produced by hybridoma technology,[1] were found to trigger immunogenic response in human and are insufficient to induce human immune effector responses.[2] To overcome these problems, chimeric, humanized and fully human mAbs were created by genetic engineering, then rituximab was approved by the US Food and Drug Administration (FDA) in 1997 as the first chimeric mAb for the treatment of B-cell non-Hodgkin's lymphoma.[3] Thereafter, a number of mAbs and Ab-based molecules such as Ab-drug conjugates (ADCs), antibody (Ab) fragments and Fc-fusion proteins have extensively developed to become the dominant products in the biopharmaceutical market.[4] mAbs approved by the FDA become 64 products in 2018.[5]

Through specific binding to target molecules on cancer cells, Abs can mediate various anti-tumor effects, including cross-linking surface antigens to induce cell death signals, blocking cell proliferation activation signals such as cetuximab (anti-epidermal growth factor receptor (EGFR) mAb) and trastuzumab (anti-human epidermal growth factor receptor-2 (HER2) mAb), antibody-dependent cellular cytotoxicity (ADCC) such as rituximab (anti-B-lymphocyte antigen CD20 mAb), complement-dependent cytotoxicity (CDC) and triggering the anti-tumor immune response[6] such as ipilimumab (anti-cytotoxic T-lymphocyte-associated protein 4 mAb)[7] and nivolumab (anti-programmed cell death protein 1 mAb)[8]. mAbs are powerful molecules for effective cancer treatment, but still have some drawbacks, for example, high molecular weight (MW), limited tissue penetration and high production cost.[9] Hence, development of small Ab alternatives such as Ab

fragments, Ab mimetics or target-binding peptides to overcome the limitation of mAbs has been desired.

1-2. Conformation of immunoglobulin G and antibody fragments

Immunoglobulin (Ig) G, most popular class of therapeutic mAbs, is a heterotetrameric glycoproteins consisting of two heavy (H) and two light (L) chains linked by disulfide bonds[10] (**Fig. 1-2-1**) with approximately 150 kDa molecular size. Both heavy and light chains contain variable (V) and constant (C) domains, which are composed of 110-130 amino acids, averaging 12–13 kDa.[11] The V domains bind antigens and the C domains specify effector functions such as activation of complement or binding to Fc receptors.[12] The antigen-binding sites, also known as hypervariable regions or complementarity determining regions (CDRs), at the tip of the Fab regions are formed by the V domains of both the H and L chains. The L chain has two domains known as V_L and C_L while heavy chain has four domains, V_H, C_{H1}, C_{H2} and C_{H3}.[13] Each domain has antiparallel curled β-sheet sandwich that is known as an Ig fold.[14]

In addition to the full-length Abs, various types of Ab fragments have been developed for clinical use.[15] For example, antigen-binding fragments (Fabs), single-chain variable fragments (scFvs), divalent and multivalent Ab fragments (i.e. diabody, tribody, tetrabody and pentabody) and heavy chain antibodies (V_{HH}) were developed base on their binding affinity, immunogenicity, half-life and effector function[16] (**Fig. 1-2-2**). There are well known Fabs approved by US FDA; ReoPro (abciximab), Lucentis (ranibizumab) and Cimzia (certolizumab pegol) are used for cardiovascular, ophthalmic and immunological indications treatments, respectively.[17] In addition, the other antibody fragments or mimetics are currently

in clinical development.

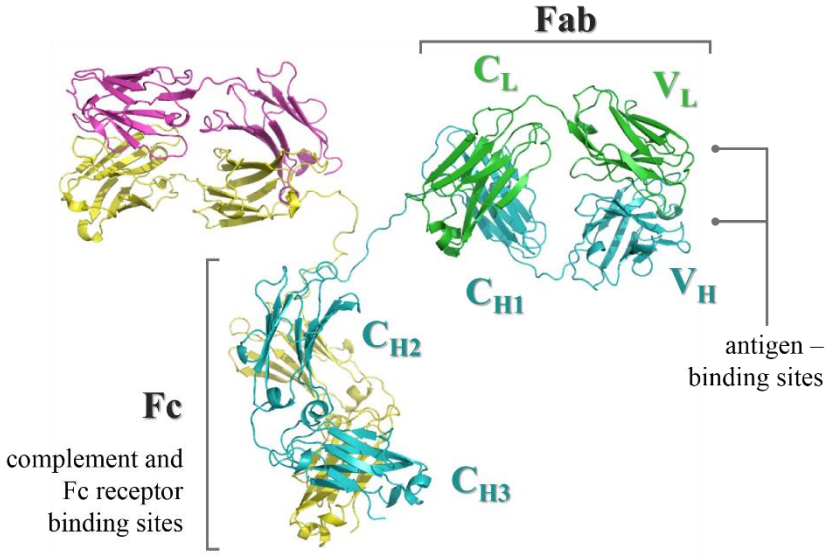

Figure 1-2-1. Conformation of IgG. H chains fold into a one V_H and either three C_H1, C_H2, C_H3 domains, whereas L chains consist of a V_L and a C_L. CDRs located at the tip of the Fab regions are formed from the variable domains of both the H and L chains. Fc region mediates interaction with effector molecules, such as complements and Fc receptors. A figure was adapted from Junda et al. (2016).[10]

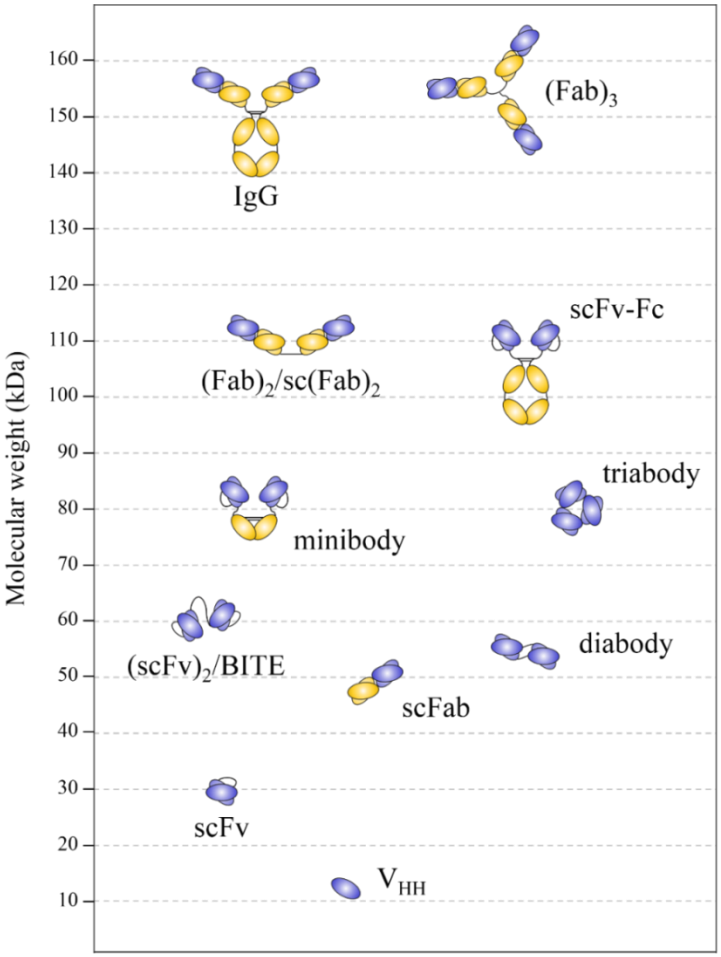

Figure 1-2-2. Schematic structure and MW of intact antibody and various genetically engineered Ab fragments. A single-domain Ab, also called nanobody, is the smallest antibody fragment consisting of one variable domain of a heavy-chain antibody (V_{HH}). V_L and V_H together form a monovalent antigen binding site called Fv and connected through a peptide linker to generate scFv. A $(scFv)_2$/BITE (bispecific T cell engager) is bispecific single-chain Abs consisting of two scFv fragments, joined via a flexible linker. Diabody and triabody fragments can be formed by spontaneous association of monovalent scFvs between V domains. The 80 kDa minibody results from the fusion of scFv to human IgG_1 C_{H3} domain. The scFv-Fc is a small IgG-like recombinant Ab (100–105 kDa) generated by fusion of a scFv with human IgG1 hinge and Fc regions (C_{H2} and C_{H3} domains). The scFab is generated by flexible linking of C_L on C-terminus to V_H on N-terminus. scFab has been multimerized to generate divalent, $(Fab)_2$/$sc(Fab)_2$ and trivalent $(Fab)_3$.[16]

1-3. Antibody mimetics and the alternatives

In addition to antibody fragments, a diverse type of antibody mimetics targeting marker proteins have been developed. The antibody mimetics are smaller (40 – 100 amino acid residues) than antibodies, often lack or less disulfide bond and have affinity constants range 1-100 nM.[18] Due to the smaller molecular size, the antibody mimetics can reduce production cost through bacterial expression system and chemical synthesis, effectively penetrate cells and tissues and be quickly eliminated from the body, which is suitable for diagnostic molecular imaging. A numbers of non-Ig molecules for development of scaffold-based antibody mimetics have been identified and some of which have already been tested in clinical trials (**Fig. 1-3-1**).[19] Until 2018, there are only three non-Ig scaffolds, ziconotide (Knottin domain scaffold), linaclotide (Knottin domain scaffold) and ecallantide (Kunitz domain scaffold) were approved by FDA for the treatments of neuropathis pain, irritable bowel disease and hereditary angioedema, respectively, while the pegdinetanib (CT-322), a human tenth fibronectin type-III (FN3)-based drug, has undergone phase II in clinical trials for the treatment of pancreatic cancer.[20]

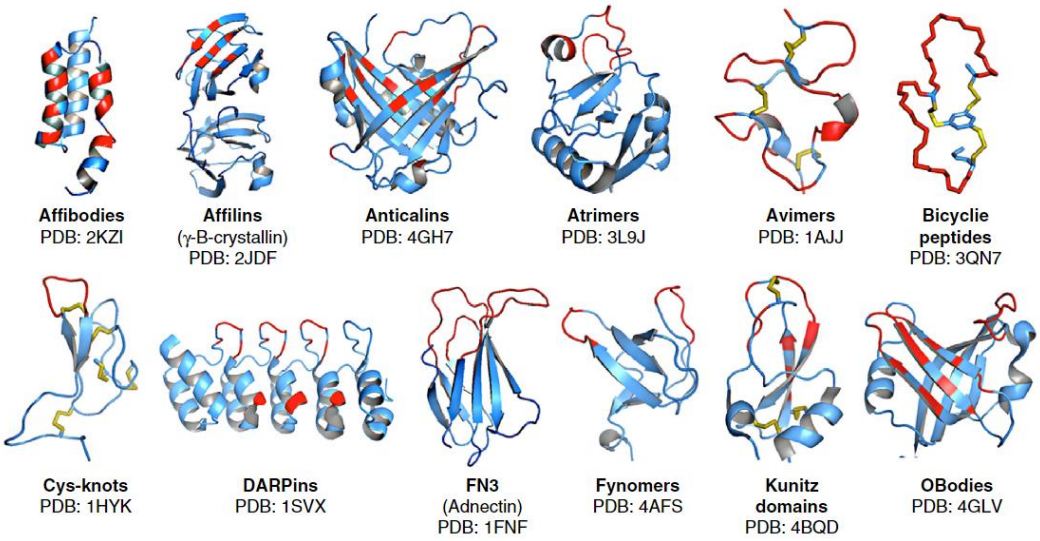

Figure 1-3-1. Non-immunoglobulin scaffolds currently used for development of novel therapeutics. Until 2018, three drugs of Kunitz and Knottin domain-based drugs have been approved by FDA. The figure was cited from reference.[20]

1-4. HER2, a biomarker and target of cancer therapy

The HER2 is a member of the HER/EGFR/ErbB receptor tyrosine kinases (TKs) family that plays vital role in human cancer.[21] The human HER family is comprised of four members: HER1 (ErbB-1), HER2 (ErbB-2), HER3 (ErbB-3) and HER4 (ErbB-4), which exist as monomers on the cell surface.[22] Binding of ligands to HER receptors induces the formation of receptor homo- or hetero-dimers, activating their tyrosine kinases,[23] then the phosphorylation of specific tyrosine residues within their cytoplasmic domain activate signaling pathways (**Fig. 1-5-1**), such as the mitogen-activated protein kinase (MAPK) and phosphatidylinositol-4,5-bisphosphate 3-kinase (PI3K) pathways, leading to cell proliferation, survival, differentiation, angiogenesis and invasion.[24]

HER2 is a transmembrane glycoprotein, consisting of 1255 amino acids with MW 185 kDa and it is encoded by HER2 gene which located on human chromosome 17. HER2 has been identified as a therapeutic target because of its role

in the progression of many cancers, including breast cancer,[25] gastric cancer[26] and ovarian cancer.[27] In line with this, two HER2-targeting mAbs have already been approved by the FDA for the treatment of HER2-positive cancers: trastuzumab for the treatment of breast cancer and gastric cancer[28] and pertuzumab for HER2-positive breast cancer.[29] Trastuzumab targets to domain IV of HER2 extracellular domain and involves in ADCC and blocking of receptor dimerization[30] (**Fig. 1-5-2**). The success of trastuzumab has promoted development of several mAb targeting HER2 receptor: Pertuzumab blocks receptor dimerization of HER2 at the different site from trastuzumab, Ado-trastuzumab emtansine is ADC and Lapatinib is reversible inhibitor of the ATP-binding site at the TK domains of EGFR or HER2.[24]

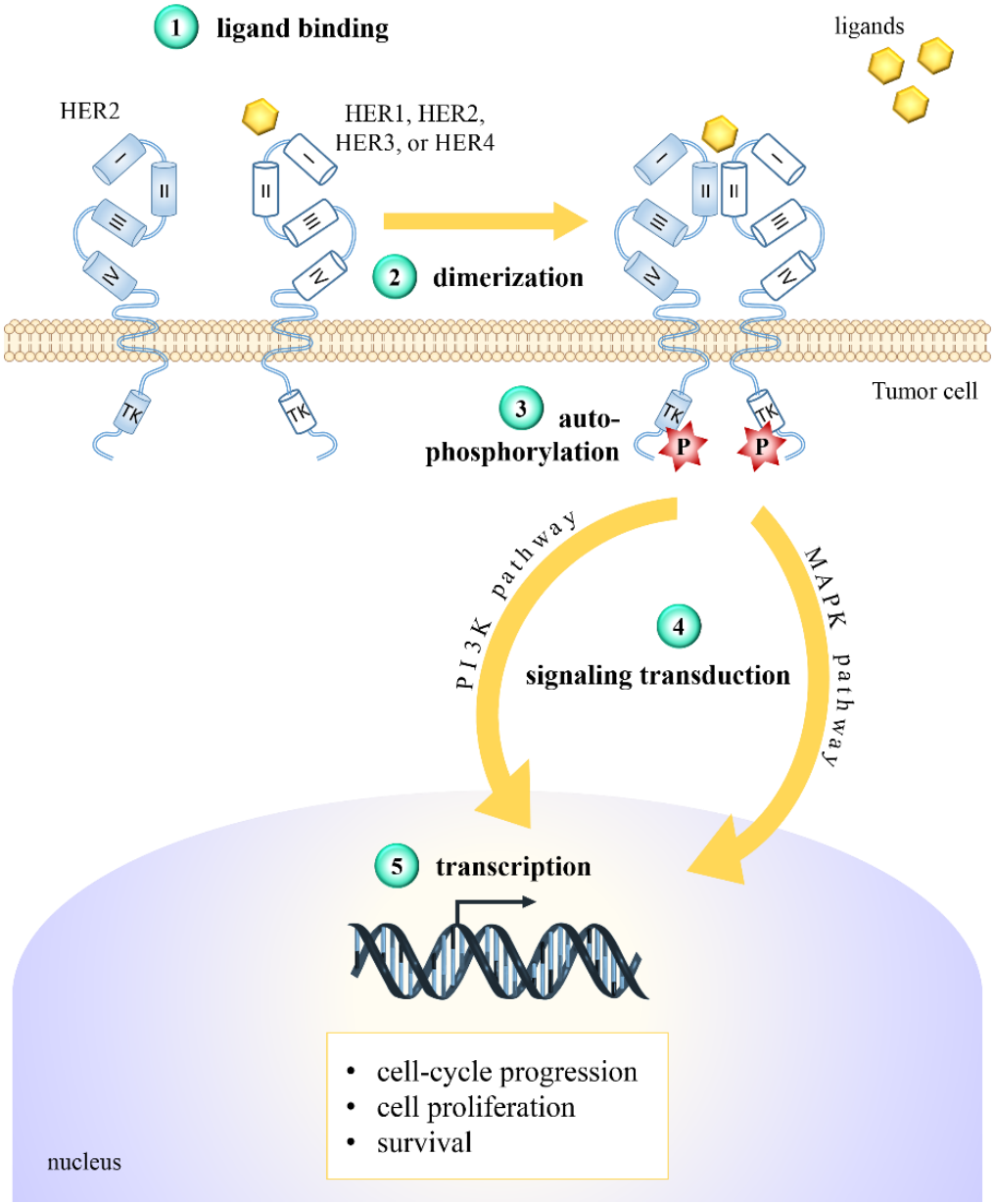

Figure 1-5-1. Signaling pathways activated by dimerization of HER receptors. Ligand binding HER receptor (step 1) initiates the formation of receptor homo- and heterodimers (step 2), leading the activation of intracellular TK domain and the autophosphorylation (step 3), which activates pivotal signaling pathways, PI3K and MAPK pathways (step 4). As a result, the signals trigger a cascade of complex cell biochemistry that regulates various cell functions such as proliferation, cell-cycle progression and survival (step 5).

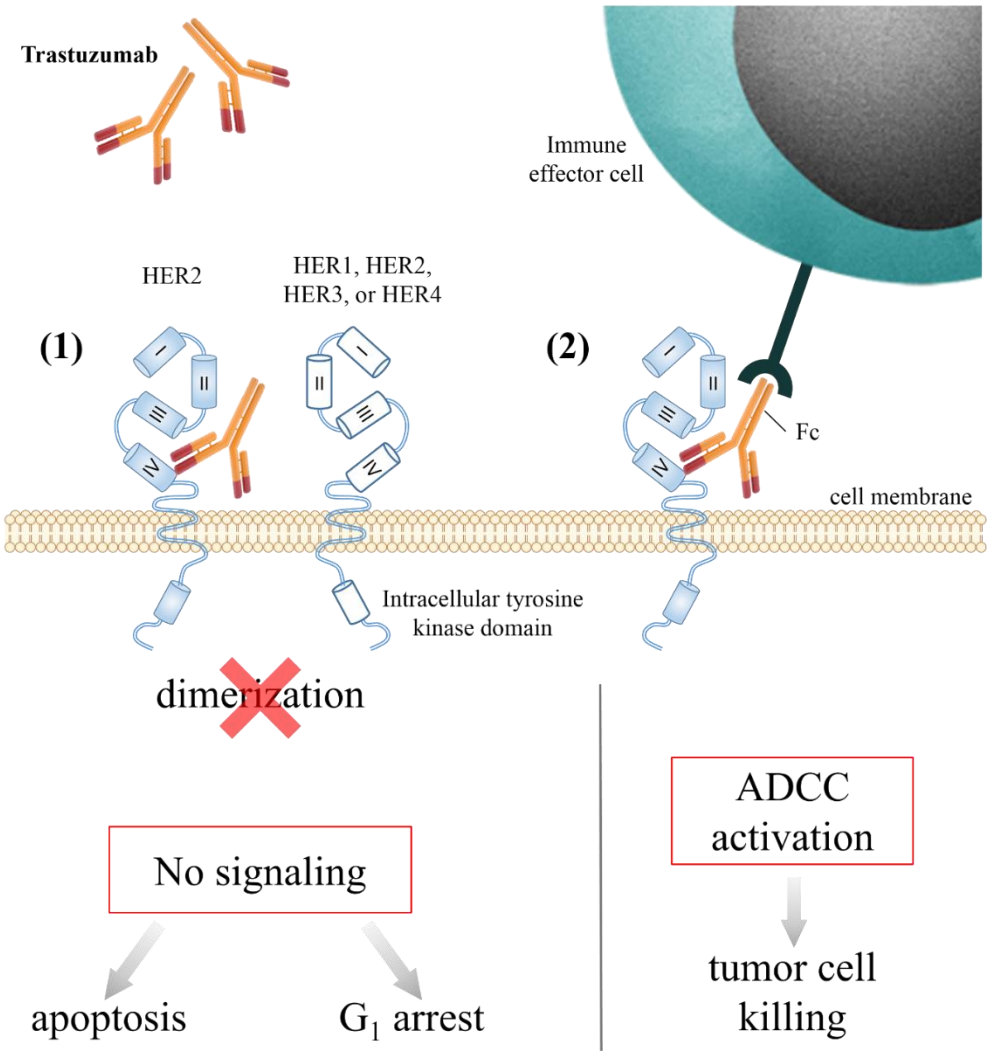

Figure 1-5-2. The mechanism of action of trastuzumab. (1) Binding of trastuzumab to HER2 prevents homo- or heterodimerization of receptors and disrupts signal transduction, inducing cell death or cell cycle arrest. (2) Trastuzumab induces tumor-cell killing by Fc receptor-mediated engagement of immune effector cells, so called ADCC effect.

1-5. Research purpose

Although mAbs and mAb fragments have become dominant therapeutic agents due to their high specificity and affinity to target molecules, they suffer from limitation in high molecular weight, limited tissue penetration and high production cost. Alternatively, target-binding peptides are small and easily prepared by chemical synthesis but their binding affinity and biological stability is low. Therefore, I am intended to develop HER2-targeting small proteins with a molecular size is in chemical synthesizable range and higher binding affinity by immobilization of binding peptides into small protein scaffolds for clinical applications.

Previous study found that the affinity and protease resistance of peptides was greatly improved after their structure was immobilized by grafting into a particular site in a protein scaffold.[31] However, this antibody mimetics is not suitable as a therapeutic drug because of its high molecular weight and exogenous origin that may cause immunogenicity. Based on this finding, a method for developing fluctuation-regulated affinity protein (FLAP) having mAb-derived peptide (AbP) was designed. This method involves the grafting of AbPs derived from trastuzumab into small scaffold proteins to immobilize AbPs structure. In addition, because the grafted peptides in FLAPs are structurally immobilized, these peptides are expected to have higher proteolysis resistance than linear peptides. Based on such hypotheses, I am aiming to develop FLAP with an immobilized HER2-binding peptide (HBP-FLAP) that has improved proteolysis resistance and exhibits specific HER2-binding properties *in vitro* and *in vivo*.

References

1. Weiner, L. M., Surana, R. & Wang, S. Monoclonal antibodies: Versatile platforms for cancer immunotherapy. *Nat. Rev. Immunol.* **10**, 317–327 (2010).
2. Brekke, O. H. & Sandlie, I. Therapeutic antibodies for human diseases at the dawn of the twenty-first century. *Nature Reviews Drug Discovery* **2**, 52–62 (2003).
3. Schrama, D., Reisfeld, R. A. & Becker, J. C. Antibody targeted drugs as cancer therapeutics. *Nat. Rev. Drug Discov.* **5**, 147–159 (2006).
4. Ecker, D. M., Jones, S. D. & Levine, H. L. The therapeutic monoclonal antibody market. *MAbs* **7**, 9–14 (2015).
5. Tsumoto, K., Isozaki, Y., Yagami, H. & Tomita, M. Future perspectives of therapeutic monoclonal antibodies. *Immunotherapy* **11**, 119–127 (2019).
6. Weiner, G. J. Monoclonal antibody mechanisms of action in cancer. *Immunol. Res.* **39**, 271–278 (2007).
7. Scott, A. M., Wolchok, J. D. & Old, L. J. Antibody therapy of cancer. *Nat. Rev. Cancer* **12**, 278–287 (2012).
8. Weiner, G. J. Building better monoclonal antibody-based therapeutics. *Nat. Rev. Cancer* **15**, 361–370 (2015).
9. Chames, P., Van Regenmortel, M., Weiss, E. & Baty, D. Therapeutic antibodies: Successes, limitations and hopes for the future. *Br. J. Pharmacol.* **157**, 220–233 (2009).
10. Janda, A., Bowen, A., Greenspan, N. S. & Casadevall, A. Ig constant region effects on variable region structure and function. *Front. Microbiol.* **7**, 1–10 (2016).

11. Dominguez, R. & Holmes, K. C. Antibody structure and function. *Focus (Madison).* **40**, 58–78 (2011).

12. Schroeder, H. W. & Cavacini, L. Structure and function of immunoglobulins. *J. Allergy Clin. Immunol.* **125**, S41–S52 (2010).

13. Carter, P. J. Potent antibody therapeutics by design. *Nat. Rev. Immunol.* **6**, 343–357 (2006).

14. Chiu, M. L., Goulet, D. R., Teplyakov, A. & Gilliland, G. L. Antibody Structure and Function: The Basis for Engineering Therapeutics. *Antibodies* **8**, 1–80 (2019).

15. Nelson, A. L. & Reichert, J. M. Development trends for therapeutic antibody fragments. *Nat. Biotechnol.* **27**, 331–337 (2009).

16. Jain, M., Kamal, N. & Batra, S. K. Engineering antibodies for clinical applications. *Trends Biotechnol.* **25**, 307–316 (2007).

17. Nelson, A. L. Antibody fragments: Hope and hype. *MAbs* **2**, 77–83 (2010).

18. Banta, S., Dooley, K. & Shur, O. Replacing Antibodies: Engineering New Binding Proteins. *Annu. Rev. Biomed. Eng.* **15**, 93–113 (2013).

19. Vazquez-Lombardi, R. *et al.* Challenges and opportunities for non-antibody scaffold drugs. *Drug Discov. Today* **20**, 1271–1283 (2015).

20. Simeon, R. & Chen, Z. In vitro-engineered non-antibody protein therapeutics. *Protein Cell* **9**, 3–14 (2018).

21. Nelson, E. L. HER2/neu: an increasingly important therapeutic target. Part 2: Distribution of HER2/neu overexpression and gene amplification by organ, tumor site and histology. *Clin. Investig. (Lond).* **4**, 705–728 (2014).

22. Zaczek, A., Brandt, B. & Bielawski, K. P. The diverse signaling network of EGFR , HER2 , HER3 and HER4 tyrosine kinase receptors and the

consequences for therapeutic approaches. *Histol Histopathol* **20**, 1005–1015 (2005).

23. Ménard, S., Pupa, S. M., Campiglio, M. & Tagliabue, E. Biologic and therapeutic role of HER2 in cancer. *Oncogene* **22**, 6570–6578 (2003).

24. Iqbal, N. & Iqbal, N. Human Epidermal Growth Factor Receptor 2 (HER2) in Cancers: Overexpression and Therapeutic Implications. *Mol. Biol. Int.* **2014**, 1–9 (2014).

25. Loibl, S. & Gianni, L. Breast cancer 2 HER2-positive breast cancer. *Lancet* **389**, 2415–2429 (2017).

26. Van Cutsem, E. *et al.* HER2 screening data from ToGA: targeting HER2 in gastric and gastroesophageal junction cancer. *Gastric Cancer* **18**, 476–484 (2015).

27. Sims, A. H. *et al.* Defining the molecular response to trastuzumab, pertuzumab and combination therapy in ovarian cancer. *Br. J. Cancer* **106**, 1779–1789 (2012).

28. Bang, Y. J. *et al.* Trastuzumab in combination with chemotherapy versus chemotherapy alone for treatment of HER2-positive advanced gastric or gastro-oesophageal junction cancer (ToGA): A phase 3, open-label, randomised controlled trial. *Lancet* **376**, 687–697 (2010).

29. Tabernero, J. *et al.* Pertuzumab plus trastuzumab and chemotherapy for HER2-positive metastatic gastric or gastro-oesophageal junction cancer (JACOB): final analysis of a double-blind, randomised, placebo-controlled phase 3 study. *Lancet Oncol.* **19**, 1372–1384 (2018).

30. Cho, H.-S. *et al.* Structure of the extracellular region of HER2 alone and in complex with the Herceptin Fab. *Nature* **421**, 756–760 (2003).

31. Kadonosono, T. *et al.* A fluorescent protein scaffold for presenting structurally constrained peptides provides an effective screening system to identify high affinity target-binding peptides. *PLoS One* **9**, e103397 (2014).

Chapter 2

Identification of small protein scaffolds and grafting acceptor sites

Abstract

The identification of adequate scaffolds and peptide-grafting sites are foremost step to discovery new Ab mimetics. According to the development of FLAPs, the suitable scaffold proteins were selected and the appropriated grafting acceptor (GA) sites were identified by computational search. The thirteen non-Ig proteins were selected as scaffold candidates and named Sca 1–13 based on their chemical synthesizable size, a low content of disulfide bonds and non-immunogenic properties. MD simulations was performed to screen and narrow down the GA candidate sites based on their properties of solvent accessibility and structurally constrained hexapeptides. Then thirteen GA sites in six scaffolds (Sca 4, 6, 8, 10, 11 and 12) were identified as suitable sites for immobilizing grafting hexapeptides with average root-mean-square fluctuation (RMSF) value less than 1.5 Å. These 13 GA sites are used for AbP grafting to generate HER2-targeting FLAPs.

2-1. Introduction

2.1.1 Molecular dynamics (MD) simulations for antibody mimetics

MD simulations is a computational method to imitate the motions of atoms in molecules of interests. MD simulation becomes an efficient tool for exploring protein motions, thermal fluctuation and structure of antigen–Ab complexes in several research fields, especially in the development of Abs or biopharmaceuticals.[1]

MD simulations can be used as a starting step for the Ab mimetics design. Force fields that are source of MD simulation such as AMBER[2] are usually utilized for confirming that the simulated system reproduces the actual motion of molecules as closely as possible. This will allow us to recapitulate *in vitro* conditions to a certain extent. *In silico* methods can be used to reduce Ab mimetics screening time by narrowing down the numbers of candidates to a select few that will be tested *in vitro*.[3]

Basically, simulation process begins with generating a computational model from the structural information provided by crystallographic or nuclear magnetic resonance data.[3] Then minimization needs to discover a stable conformation, followed by equilibration to confirm that the conformation is in equilibrium with the simulation conditions.[4,5] Finally, the simulation is performed by moving the atoms according to the equation of motion for a certain period of time. Simulation results can be used to predict or analyze several properties of the molecule, such as conformational change, fluctuation and binding energies.

In order to develop FLAP, the scaffold proteins were first selected by computational search and the GA sites for grafting the hexapeptides were identified by MD simulation.

2-2. Materials and Methods

2-2-1. MD simulations

The initial coordinates of nine scFv molecules and 13 scaffolds were taken from PDB accession codes 2YC1, 3JUY, 3UX9, 4BUH, 4KV5, 4UT7, 4X4X, 5C2B and 5D9Q, and 4HSV, 4ZAI, 2QKQ, 3UA7, 2YUU, 2RGF, 3TSV, 1TTG, 3FIA, 4EN3, 1WGR, 3PGF and 4DZ8, respectively. The structures of linear CDR peptides, model linear peptides, model hexapeptide-grafting scFv molecules and model hexapeptide-grafting scaffold candidates were generated using Discovery studio 3.1 (Accelrys, San Diego, CA, USA). The systems were optimized via energy minimization and equilibrated with backbone restraints. Production runs were performed for at least 10 ns for trajectory analysis. All MD simulations were performed using the Amber 14 and 16 program packages[6] on TSUBAME (Global Scientific Information and Computing Center, Tokyo Institute of Technology). The Amber ff14SB force field and the GB/SA implicit solvent model were used. The time-step for MD simulations was set to 2 fs with the SHAKE algorithm. A nonbonded cutoff of 999.9 Å was used. The temperature was kept constant at 300 K using the Berendsen rescaling method.

The root-mean-square fluctuations (RMSFs) during the final 5 ns of each production run were calculated to investigate the backbone fluctuations in each system using the cpptraj module. The solvent accessible surface areas (SASAs) of the final structures of each production run were calculated to identify the solvent-accessible residues in the 13 scaffolds using the cpptraj module.

2-2-2. Identification of GA sites

The GA sites were identified via an *in silico* two-step method. Firstly, the constrained and solvent accessible (CSA) hexapeptides were selected based on particular characteristics. The following filters were applied to narrow down the potential hexapeptides:

1. The hexapeptides were from a loop region sequentially flanked by α-helices, β-strands or disulfide-bonded cysteine residues.
2. The buried SASA of each residue was larger than 15 $Å^2$.
3. The average RMSF of the hexapeptides was less than 1.0 Å.

Next, each CSA hexapeptide in the scaffolds was computationally replaced with 20 different homo-hexapeptides, including Ala-Ala-Ala-Ala-Ala-Ala (A6), Cys-Cys-Cys-Cys-Cys-Cys (C6), Asp-Asp-Asp-Asp-Asp-Asp (D6), Glu-Glu-Glu-Glu-Glu-Glu (E6), Phe-Phe-Phe-Phe-Phe-Phe (F6), Gly-Gly-Gly-Gly-Gly-Gly (G6), His-His-His-His-His-His (H6), Ile-Ile-Ile-Ile-Ile-Ile (I6), Lys-Lys-Lys-Lys-Lys-Lys (K6), Leu-Leu-Leu-Leu-Leu-Leu (L6), Met-Met-Met-Met-Met-Met (M6), Asn-Asn-Asn-Asn-Asn-Asn (N6), Pro-Pro-Pro-Pro-Pro-Pro (P6), Gln-Gln-Gln-Gln-Gln-Gln (Q6), Arg-Arg-Arg-Arg-Arg-Arg (R6), Ser-Ser-Ser-Ser-Ser-Ser (S6), Thr-Thr-Thr-Thr-Thr-Thr (T6), Val-Val-Val-Val-Val-Val (V6), Trp-Trp-Trp-Trp-Trp-Trp (W6) and Tyr-Tyr-Tyr-Tyr-Tyr-Tyr (Y6), after which MD simulations of each structure was calculated. CSA hexapeptides in which the average RMSF of all replaced homo-hexapeptides was less than 1.5 Å were identified as GA sites.

2-3. Results

2-3-1. Selection of small protein scaffold candidates

In order to develop FLAPs, the small protein scaffolds were first computational selected. Ideal traits of scaffold candidates for drug development include a suitable size (less than 120 amino acids) that allows straightforward chemical synthesis, a low number of disulfide bonds and non-immunogenicity. Taking these traits into consideration, 13 non-Ig proteins of less than 104 amino acids in length that contained fewer than two disulfide bonds as scaffold candidates from endogenous proteins were selected and named Sca1-Sca13, in which the numbering was assigned in order of their amino acid length **(Table 2-3-1)**.

To determine the suitable amino acid length of grafting peptides, a length distribution of antigen-binding contiguous sequences in various Abs were analyzed. The longest contiguous sequence of antigen-contact residues in 99% of antibody light chains and 93% of antibody heavy chains is six amino acids (hexapeptide) **(Fig. 2-3-1)**. Therefore, hexapeptides were selected from antibody CDR loops for grafting to the scaffolds.

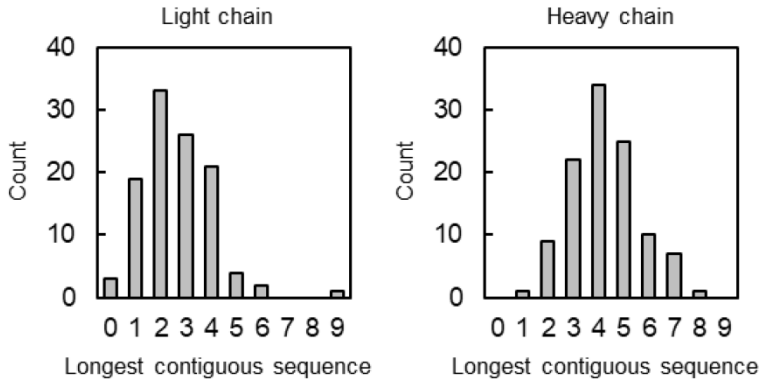

Fig. 2-3-1. Length distribution of antigen-binding contiguous sequences in various antibodies. The longest contiguous sequences that interact with antigen molecules in light (left) and heavy (right) chains were counted. The binding information of 109 antibody–antigen complexes was collected by a previous study.[7]

Table 2-3-1. List of scaffold candidates

Scaffold candidate	Protein/domain/peptide name	Structural annotation	PDB ID	Region	Length	No. of SS bond
Sca1	CXCL4L1	Small cytokines	4HSV	9−54	46	2
Sca2	CXCL13	Small cytokines	4ZAI	10−55	46	2
Sca3	SAM domain of ephrin type-B receptor 4	Orthogonal bundle	2QKQ	908−968	61	0
Sca4[a]	SH3 domain of Fyn	Others	3UA7	81−143	63	0
Sca5	C1 domain of protein kinase C	Others	2YUU	1−83	83	0
Sca6[a]	Ras-binding domain of RalGEF	Roll	2RGF	11−97	87	0
Sca7	PDZ domain of ZO-1 MAGUK	Roll	3TSV	420−512	93	0
Sca8[a]	Fibronectin type III domain	Immunoglobulin-like	1TTG	1−94	94	0
Sca9	EH1 domain of intersectin-1	Orthogonal bundle	3FIA	6−103	98	0
Sca10[a]	β2-Microglobulin	Immunoglobulin-like	4EN3	1−99	99	1
Sca11[a]	Growth factor receptor-bound protein 7	Roll	1WGR	1−100	100	0
Sca12[a]	Constant region of IgG-light chain (CL)	Immunoglobulin-like	3PGF	111−213	103	0
Sca13	Constant region of IgG-heavy chain (CH2)	Immunoglobulin-like	4DZ8	238−341	104	1

[a] These scaffolds have GA sites.

2-3-2. Determination of the criteria for hexapeptide-grafting sites in scaffolds

The structures of the 13 non-Ig scaffolds were equilibrated using MD simulations. The 185 hexapeptides flanked by α-helices, β-strands or disulfide-bonded cysteine residues in the scaffolds were selected as candidate sites for substitution with CDR-derived hexapeptides and their solvent accessibility was determined by measuring their buried SASA (**Fig. 2-3-2-1**). The hexapeptides with a SASA value of greater than 15 $Å^2$ for each residue were selected as solvent accessible (SA) hexapeptides. As a result, the 185 possible sites were reduced to 69 hexapeptides-grafting candidate sites.

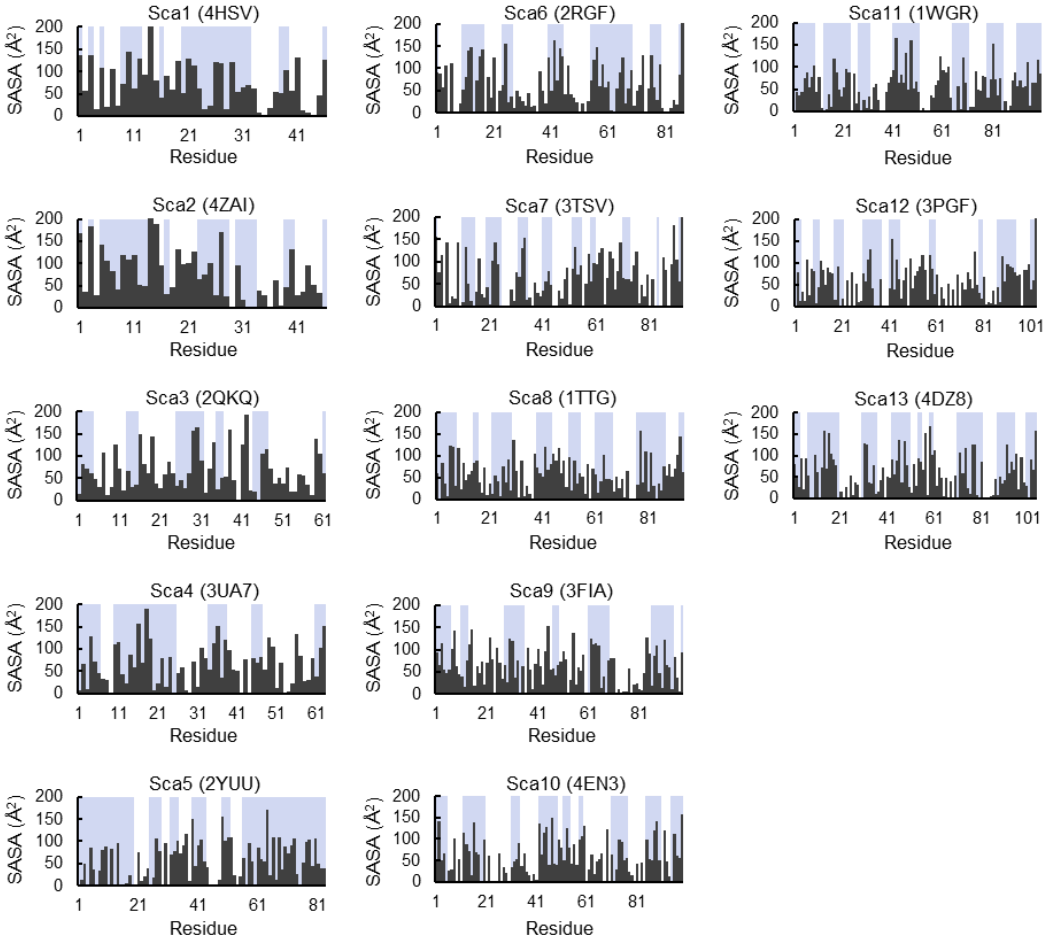

Figure 2-3-2-1. SASA calculation of scaffolds. The SASA values of 13 scaffolds were calculated and are shown by residue. The loop regions are highlighted by light blue.

To select ideal grafting sites that enable the grafted hexapeptide to be structurally constrained, the 69 candidate sites were computationally evaluated using our original criteria. The atomic fluctuation of each CDR hexapeptide was evaluated using publicly available structural data from nine single chain Fv (scFv) fragment antibodies and used to determine the appropriate criteria. Since the CDR loop of an antibody is immobilized by framework regions (FRs), these regions are the best suited for determining appropriate criteria for the immobilized state of peptides. The most flexible hexapeptide sequence (Flex-CDR hexapeptide) in each CDR was determined based on the RMSF values of all hydrogen-free atoms calculated using the trajectories of MD simulations (**Fig. 2-3-2-2**). As a comparison to the highly fluctuating hexapeptides, the RMSF values of linear hexapeptides with the same amino acid sequences as the Flex-CDR hexapeptides were also calculated. These calculations showed that the average RMSF values of the linear hexapeptides were mostly more than 1.5 Å (47/53), whereas the average RMSF values of the hexapeptides in the scFv were mostly less than 1.5 Å (51/53) (**Fig. 2-3-2-3**). Therefore, the criterion used for identifying structurally constrained hexapeptides was an average RMSF value of less than 1.5 Å.

2YC1

H1: GFTFDN YAMH
H2: GI SRSSGD IDYADSVKG
H3: G GVGSFD T

L1: RA SQSVRS YLA
L2: D ASNRAT
L3: QQ YRYSPR T

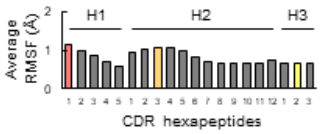

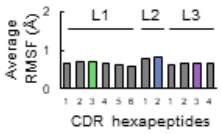

3JUY

H1: GYRFSH FTVH
H2: WINPYNGNKEF SAKFQD
H3: VGEW GWDDSP YDNYYMDV

L1: R SSHSIR SRRVA
L2: G VSNRAS
L3: QVY GASSYT

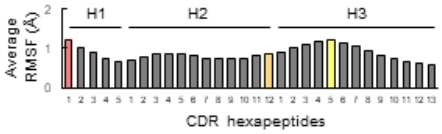

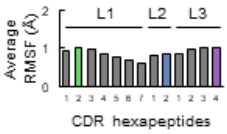

3UX9

H1: GFTFSS YAMS
H2: AIS GSGGST YYADSVKG
H3: YIDFGD HMDF

L1: SG SSSNIG SNYVS
L2: D NNQRPS
L3: QVR DNNENE WV

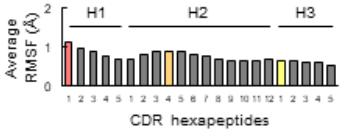

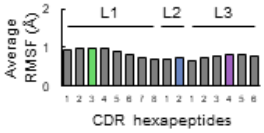

4BUH

H1: EYSFPN YWIA
H2: MIYPGDSDTRY SRSFQG
H3: LG GQLWNS YYYYYYMDV

L1: SG SSSNIG GNTVN
L2: K NNQRPS
L3: EAW DGGLRG GV

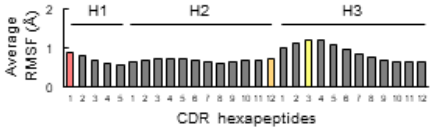

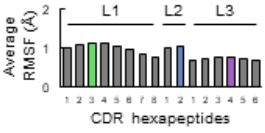

4KV5

H1: GYTFSS NVIS
H2: GV IPIVDI ANYAQRFKG
H3: T LGLVLD AMDY

L1: RAS QSLGSS YLA
L2: G ASSRAP
L3: QQ YADSPI T

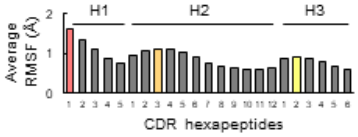

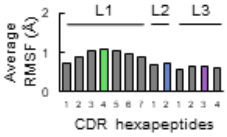

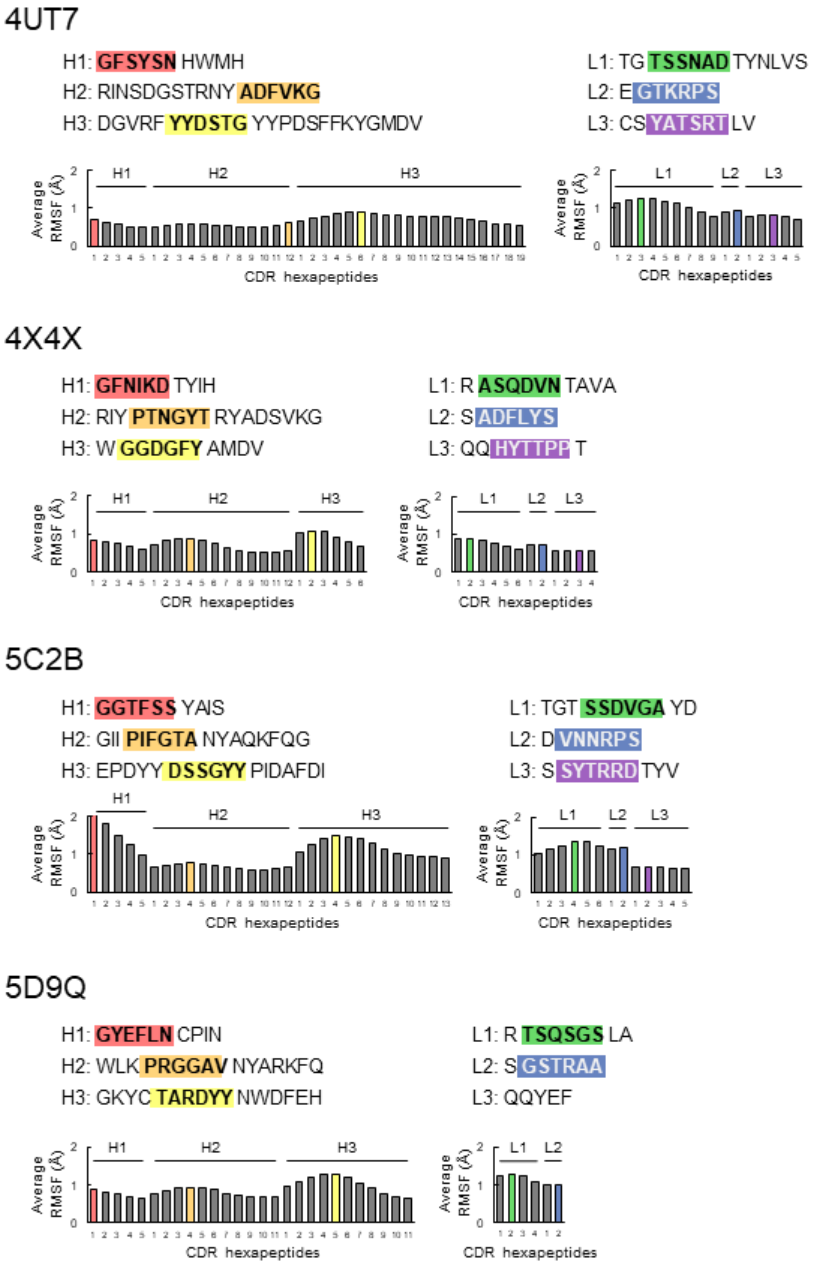

Figure 2-3-2-2. Structural fluctuation of CDRs in antibodies. Nine scFv fragment antibodies indicated by PDB ID were analyzed to investigate the atomic fluctuation of CDR hexapeptides. Amino acid sequences of six CDR loops (H1, H2, H3, L1, L2 and L3) are shown at the top of each panel. The average RMSF values of CDR-derived hexapeptides in scFv structures were calculated and are shown in the graphs under the corresponding amino acid sequences. The most flexible hexapeptides in CDR-H1, -H2, -H3, -L1, -L2 and -L3 (Flex-CDR hexapeptides) are highlighted by red, orange, yellow, green, blue and purple, respectively. Since CDR-L3 of the 5D9Q antibody is only five amino acids in length, the average RMSF values for this peptide are not shown.

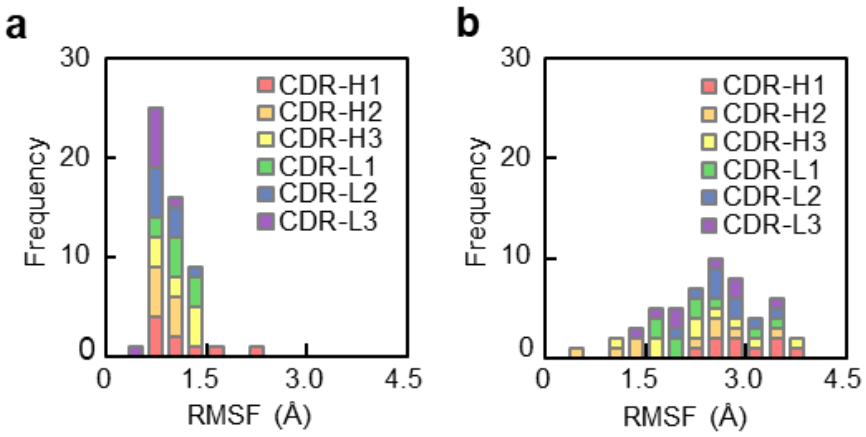

Figure 2-3-2-3. Peptide-immobilizing effect of an antibody. (a) Fluctuation of CDR peptides in antibody scFv. The average RMSF values of 53 CDR hexapeptides in nine scFv structures from PDB are shown in the graph. (b) Fluctuation of CDR-derived linear peptides. The average RMSF values of 53 CDR-derived linear peptides that possess the same amino acid sequences as the peptides in (a) are shown in the graph.

After applying the above selection criterion, 60 out of 69 sites were found to potentially immobilize a grafted hexapeptide (average RMSF < 1.5 Å), and 18 out of these 60 sites were identified with the potential to highly immobilize a hexapeptide (average RMSF < 1.0 Å). This subset of 18 hexapeptides was named the CSA hexapeptides, and each CSA hexapeptide was named Sca4-1–Sca12-1 to indicate the scaffold in which it is located and its position from the N-terminus (**Fig. 2-3-2-4** and **Table 2-3-2**). The 18 CSA hexapeptides, which are potential substitution sequences for antigen binding hexapeptide, within the 7 scaffolds were evaluated further to identify ideal substitution sites.

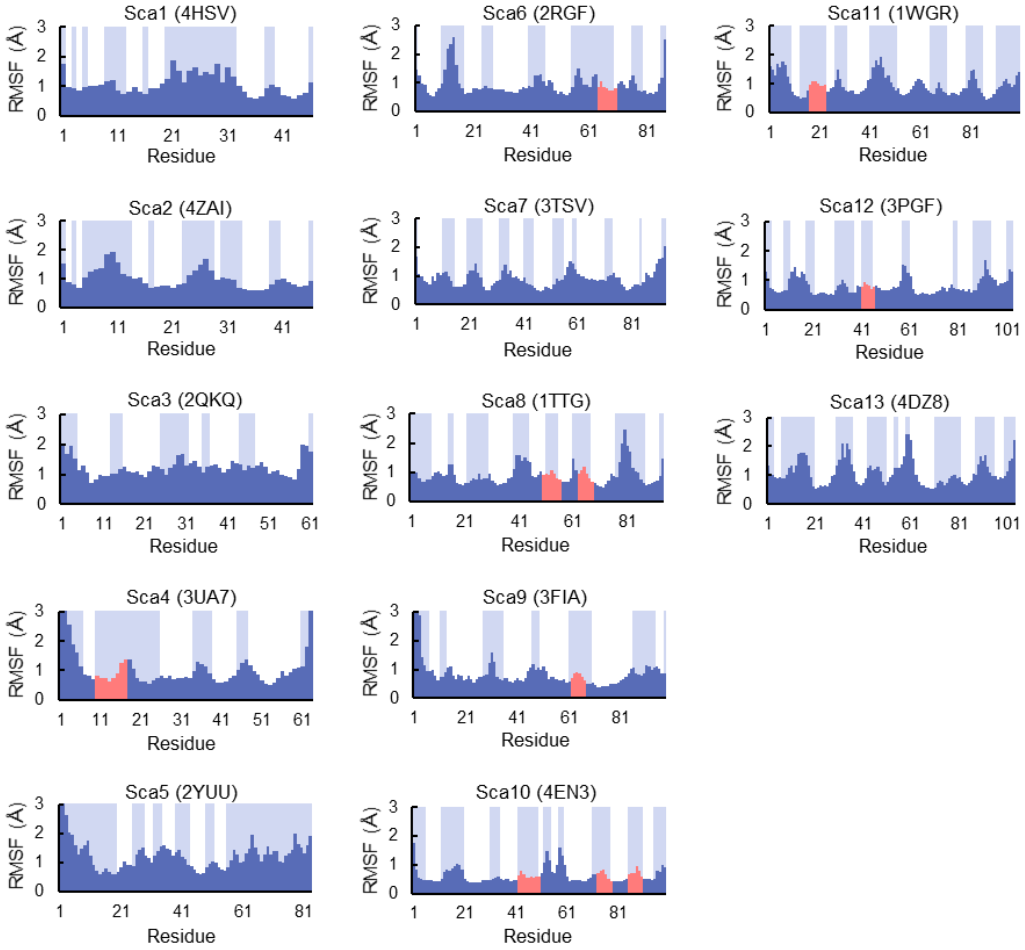

Figure 2-3-2-4. RMSF calculation of scaffolds. The RMSF values of 13 scaffolds were calculated and are shown by residue. The amino acid residues for 18 CSA hexapeptides are shown by pink-colored bars. Loop regions are highlighted in light blue.

Table 2-3-2. Average RMSF and SASA of CSA hexapeptides

CSA hexapeptide [region]	Average RMSF (Å)	SASA (Å^2)					
		1	2	3	4	5	6
Sca4-1 [90−95][a]	0.76	109	116	44	22	86	57
Sca4-2 [91−96]	0.83	116	44	22	86	57	156
Sca4-3 [92−97]	0.93	44	22	86	57	156	69
Sca6-1 [74−79][a]	0.84	56	92	124	22	54	97
Sca6-2 [75−80][a]	0.83	92	124	22	54	97	15
Sca8-1 [50−55][a]	0.93	28	96	19	88	36	59
Sca8-2 [51−56][a]	0.91	96	19	88	36	59	53
Sca8-3 [63−68][a]	0.95	42	101	47	47	44	16
Sca9-1 [67−72]	0.79	126	112	115	108	15	39
Sca10-1 [42−47]	0.63	137	64	115	127	39	150
Sca10-2 [43−48][a]	0.62	64	115	127	39	150	41
Sca10-3 [44−49][a]	0.58	115	127	39	150	41	39
Sca10-4 [45−50][a]	0.57	127	39	150	41	39	98
Sca10-5 [73−78][a]	0.66	30	99	94	50	56	24
Sca10-6 [85−90][a]	0.74	97	53	49	120	141	51
Sca11-1 [17−22]	1.00	120	89	50	33	55	95
Sca11-2 [18−23][a]	0.99	89	50	33	55	95	87
Sca12-1 [151−156][a]	0.80	40	154	39	106	63	18

[a] These hexapeptides correspond to GA sites.

2-3-3. Validation of grafting sites that immobilize a grafted hexapeptide

In developing a method to validate the potential of the CSA hexapeptides as ideal hexapeptide-grafting sites, it was hypothesized that an ideal hexapeptide-grafting site could immobilize any hexapeptide structure. To test this hypothesis, Flex-CDR hexapeptides in two scFv were replaced with 20 different homo-hexapeptides and the average RMSF values of the grafted hexapeptides were profiled (RMSF profiling). The homo-hexapeptides included the smallest (Gly-Gly-Gly-Gly-Gly-Gly; G6), bulkiest (Trp-Trp-Trp-Trp-Trp-Trp; W6), most hydrophobic (Ile-Ile-Ile-Ile-Ile-Ile; I6), most acidic (Glu-Glu-Glu-Glu-Glu-Glu; E6) and most basic (Arg-Arg-Arg-Arg-Arg-Arg; R6) peptides among the 6.4×10^7 theoretical hexapeptide species. Therefore, these peptides would be ideal models to validate scaffolds for resistance to all possible factors that may be problematic in immobilizing peptides, such as weak atomic forces, repulsion forces and steric hindrances. RMSF profiling revealed that the majority of the average RMSF values of the linear homo-hexapeptides were greater than 2 Å, whereas the average RMSF values of all the homo-hexapeptides grafted into scFv were 1.5 Å or less (**Fig. 2-3-3-1**). These findings indicate that a method for selecting ideal scaffolds using 20 different homo-hexapeptides is valid.

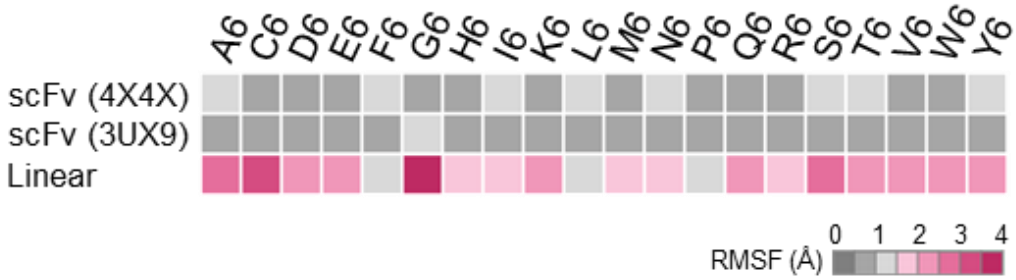

Figure 2-3-3-1. RMSF profiling of antibodies. RMSF profiling of Flex-CDR hexapeptides in scFv scaffolds and linear hexapeptides. Two CDR-H3 loops of scFv proteins (PDB ID: 4X4X and 3UX9) and one computationally-generated linear hexapeptide were profiled. Hexapeptides with average RMSF values of less or more than 1.5 Å are shown by gray- or magenta-colored squares, respectively.

RMSF profiling revealed that 13 out of the 18 CSA hexapeptides in six scaffolds have an average RMSF value of less than 1.5 Å (**Fig. 2-3-3-2a, Tables 2-3-1** and **2-3-2**), indicating that these sites have high potential to immobilize the structure of any grafted hexapeptide. The structural features of these 13 CSA hexapeptides, hereinafter referred to as graft acceptor (GA) sites, were then analyzed. Interestingly, a half of the scaffolds with GA sites (Sca4, Sca6, Sca8, Sca10, Sca11 and Sca12) have multiple GA sites (**Tables 2-3-1** and **2-3-2**). These GA sites were classified according to their adjoining secondary structures. They tended to appear in the strand-loop-strand motifs of scaffolds (**Fig. 2-3-3-2b**). Next, the influence of peptide deflection on fluctuation was evaluated by analyzing the distribution of distances between the Cα atoms of the first and sixth amino acids of GA sites. The results indicate that the distances between the Cα atoms of GA sites are distributed widely, suggesting that the presence of GA sites is independent of the peptide deflection (**Fig. 2-3-3-2c**).

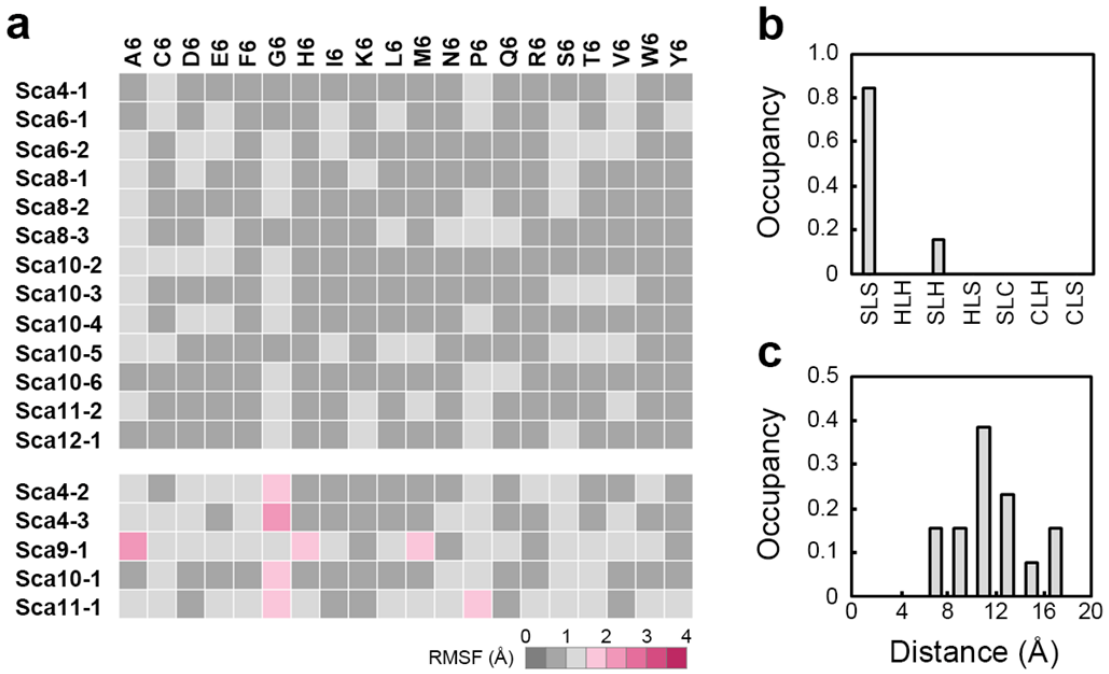

Figure 2-3-3-2. The effect of scaffolds on peptide immobilization. (a) RMSF profiling of 18 CSA hexapeptides. Average RMSF values of less or more than 1.5 Å are shown by grey- or magenta-colored squares, respectively. (b) Structural motifs of the flanked loops containing the GA sites. SLS, strand-loop-strand; HLH, helix-loop-helix; SLH, strand-loop-helix; HLS, helix-loop-strand; SLC, strand-loop-cysteine; CLH, cysteine-loop-helix; CLS: cysteine-loop-strand. (c) Distance distribution between Cα atoms of the first and sixth amino acids of hexapeptides in the GA sites.

Discussion

In this chapter, the selection of small scaffold proteins by computational search and the identification of GA sites by MD simulation were described. To develop FLAPs, I initially selected 13 non-Ig human protein scaffold candidates that had sizes amenable to chemical synthesis and a low number of disulfide bonds, and then identified six suitable proteins using the validation method. After evaluating all candidate GA sites with MD simulation, 13 GA sites in 6 scaffolds were identified as appropriate sites for hexapeptide immobilization. These 13 GA sites were then used to develop FLAPs in next chapters.

Among six scaffolds, two are well-studied non-Ig scaffold proteins, the SH3 domain of Fyn (Sca4, fynomer) and the fibronectin type III domain (Sca8, FN3 or adnectin) (Fig. 2-3-3-2, Tables 2-3-1 and 2-3-2), suggesting that our strategy is a very effective method for screening practical non-Ig scaffold proteins. These two domains have relatively high melting transitions (T_m = 72 °C for fynomer and 84 °C for FN3), low immunogenicity and their biodistribution can be improved by Fc-fusion and PEGylation techniques. Thus, many mutant proteins have been developed using these domains as scaffolds and some are under clinical evaluations for the treatment of cancer, hypercholesterolemia, cachexia and plaque psoriasis.[8,9] As FLAPs with these scaffolds are suitable for clinical application, they will be used in future research to advance to FLAPs development for clinical application.

Characterization of the other four scaffolds (Sca6, ras-binding domain of RalGEF; Sca10, beta 2-microglobulin; Sca11, growth factor receptor-bound protein 7; Sca12, constant region of IgG-light chain (C_L)) for clinical applications has received less attention. Only thermal stability is known for Sca10 (T_m = 60 °C) and Sca12 (T_m = 53 °C for murine C_L domain).[10,11] Although future studies need to

verify whether these scaffolds are suitable for clinical application, they were shown to be potential candidates for use as non-Ig scaffolds.

References

1. Yamashita, T. Toward rational antibody design: Recent advancements in molecular dynamics simulations. *Int. Immunol.* **30**, 133–140 (2018).
2. Wang, J., Wolf, R. M., Caldwell, J. W., Kollman, P. A. & Case, D. A. Development and Testing of a General Amber Force Field. *J. Comput. Chem.* **25**, 1157–1174 (2004).
3. Durrant, J. D. & McCammon, J. A. Molecular dynamics simulations and drug discovery. *BMC Biol.* **9**, 71 (2011).
4. Mackay, D. H. J., Cross, A. J. & Hagler, A. T. The Role of Energy Minimization in Simulation Strategies of Biomolecular Systems. *Predict. Protein Struct. Princ. Protein Conform.* 317–358 (1989). doi:10.1007/978-1-4613-1571-1_7
5. Walton, E. B. & VanVliet, K. J. Equilibration of experimentally determined protein structures for molecular dynamics simulation. *Phys. Rev. E - Stat. Nonlinear, Soft Matter Phys.* **74**, 1–8 (2006).
6. Case, D. A. *et al. Amber 2017*. *University of California, San Francisco* (2017). doi:citeulike-article-id:2734527
7. Stave, J. W. & Lindpaintner, K. Antibody and Antigen Contact Residues Define Epitope and Paratope Size and Structure. *J. Immunol.* **191**, 1428–1435 (2013).
8. Orlova, A. *et al.* Tumor imaging using a picomolar affinity HER2 binding Affibody molecule. *Cancer Res.* **66**, 4339–4348 (2006).
9. Kumar, S. R., Quinn, T. P. & Deutscher, S. L. Evaluation of an 111in-radiolabeled peptide as a targeting and imaging agent for ErbB-2 receptor-expressing breast carcinomas. *Clin. Cancer Res.* **13**, 6070–6079 (2007).

10. Geng, L. *et al.* HER2 targeting peptides screening and applications in tumor imaging and drug delivery. *Theranostics* **6**, 1261–1273 (2016).

11. Yang, X. *et al.* Peptide probes derived from pertuzumab by molecular dynamics modeling for HER2 positive tumor imaging. *PLoS Comput. Biol.* **13**, e1005441 (2017).

Chapter 3

Development of FLAPs using HER2-binding peptide derived from anti-HER2 monoclonal Abs

Abstract

mAbs bind to the antigen through their complementarity-determining regions (CDRs). Small stable proteins containing structurally immobilized CDRs are promising alternatives to mAbs. This chapter describes an efficient method to create such proteins, named fluctuation-regulated affinity proteins (FLAPs). In chapter 2, thirteen GA sites that efficiently immobilize the grafted peptide structure were initially selected from six small protein scaffolds by computational identification. For this chapter, five mAb-derived peptides (AbPs) against HER2 breast cancer marker were extracted from clinically used anti-HER2 mAbs, trastuzumab and pertuzumab, then grafted to the selected scaffolds. The combination of five CDR peptides and 13 GA sites in six scaffolds revealed that three out of the 65 combinations showed specific binding to HER2 with dissociation constants (K_D) of 24–65 nM in ELISA and 270–350 nM in biolayer interferometry. Hereinafter, the three candidates are called AbP-FLAPs. All AbP-FLAPs have FN3-based scaffold and bind to the same epitope as trastuzumab. In addition, they specifically bound to HER2 and hardly bound to EGFR, which belongs to the same receptor family as HER2. Thus, the present strategy is a promising and practical method for developing small antibody mimetics.

3-1. Introduction

3.1.1 The design strategy of antibody mimetics

Chemically synthesized small antibody mimetics (maximally around 120 amino acid in length[1]) that specifically bind to the same epitopes as their parental mAb drugs provide promising options for molecular-targeted therapies. Low-molecular-weight proteins have good tissue penetration, a high excretion rate and low production costs. Thus, in recent years, a variety of small non-Ig proteins have been generated via affinity selection of protein libraries that present randomized amino acids on the surface of non-Ig scaffold proteins.[2–7] In parallel, antibody fragmentation technologies have successfully developed small antibody mimetics. However, current design strategies for reducing mAb size are limited to the generation of 30 kDa fragment antibodies, which is still too large for practical chemical synthesis.[8] Computational protein design that rationally extracts protein fragments from large protein libraries makes it possible to more efficiently create small antigen-binding proteins with higher affinity for epitopes.[9]

3-1-2. CDR grafting technique for creation of antibody mimetics

The antigen-binding surface of mAbs is often composed of six CDRs, spread across the V_H and V_L domains. CDR-grafting techniques have been commonly used to humanize exogenous antibodies to reduce their immunogenicity.[10] A typical grafting protocol for antibody humanization includes the identification of antigen-binding regions in the parental antibody, the selection of a framework region (FR) for providing structural support to the grafted CDRs attached to the human antibody, and, finally, the optimization of amino acid residues outside of the grafted CDRs to restore or improve the affinity of the humanized antibody.[11] In a similar way, small

antibody mimetics targeting lysozyme have been generated by grafting CDRs from a single domain antibody to non-Ig scaffolds, including neocarzinostatin,[12] ubiquitin[13] and Affitins.[14] Although theses mall antibody mimetics have the same CDRs as the parental Ab, they showed various affinities for lysozyme (K_D = 0.5–230 μM), indicating that the scaffolds affect the affinity of the grafted CDRs. Therefore, when designing high-affinity antibody mimetics for practical use, it is extremely important both to select appropriate non-Ig scaffolds and to determine the proper peptide sequences in the CDRs.

In this chapter, FLAPs with AbPs were designed and evaluated. Five AbPs derived from trastuzumab and pertuzumab were independently grafted into 13 GA sites identified in chapter 2, resulting in 65 combinations. They were evaluated for specific binding to HER2.

3-2. Materials and Methods

3-2-1. MD simulations

The initial coordinates of six scaffolds were taken from PDB accession codes 3UA7, 2RGF, 1TTG, 4EN3, 1WGR and 3PGF, respectively. The CDR peptide-grafting scaffolds were generated using Discovery studio 3.1 (Accelrys, San Diego, CA, USA). The systems were optimized via energy minimization and equilibrated with backbone restraints. Production runs were performed for at least 10 ns for trajectory analysis. All MD simulations were performed using the Amber 16 program packages[15] on TSUBAME (Global Scientific Information and Computing Center, Tokyo Institute of Technology). The Amber ff14SB force field and the GB/SA implicit solvent model were used. The time-step for MD simulations was set to 2 fs with the SHAKE algorithm. A nonbonded cutoff of 999.9 Å was used. The temperature was kept constant at 300 K using the Berendsen rescaling method.

The RMSFs during the final 5 ns of each production run were calculated to investigate the backbone fluctuations in each system using the cpptraj module.

3-2-2. Identification of antigen-binding CDR hexapeptides

Antigen-binding CDR hexapeptides of mAbs were identified using the *in silico* alanine hexapeptide scanning method. The binding energies of trastuzumab and pertuzumab toward HER2 in their complex structures (PDB accession codes 1N8Z and 1S78, respectively) were predicted by calculating the total energy difference after energy minimization and equilibration using the Amber ff14SB force field between bound and unbound structures, referred to as ΔG scores. Each CDR-derived hexapeptide sequence was computationally mutated to an alanine hexapeptide and the top three and two sequences of trastuzumab and pertuzumab,

respectively, with ΔG scores that decreased by at least 23 kcal/mol after alanine hexapeptide mutation were selected.

3-2-3. Grafting of antigen-binding CDR hexapeptides onto scaffolds

The antigen-binding CDR hexapeptides were computationally grafted into scaffolds to generate FLAP candidates by replacing the residues of GA sites in the scaffolds with corresponding residues of the CDR hexapeptides. Structures were optimized by MD simulations of each FLAP candidate. The heavy-atom RMSD of the grafted CDR hexapeptides between the peptides in the antibody CDR and those in the FLAP candidates was calculated from crystal structures of the antibodies and predicted structures of the FLAP candidates using the cpptraj module.

3-2-4. Plasmid construction and expression of FLAP candidates

The cDNA encoding fusion proteins composed of a His-tag, *Renilla* luciferase 8.6-535 (RLuc), GGGS linker and scaffolds (in this order) used for bioluminescence imaging (BLI)-ELISAs or the cDNA encoding His-tagged scaffolds used for ELISA were inserted into the multi-cloning site of the pGEX-6P-3 plasmid (GE Healthcare, Little Chalfont, UK) by the Gibson assembly technique (New England Biolabs, Ipswich, MA, USA). The cDNA encoding FLAP candidates were constructed by site-directed mutation of scaffold sequences. These plasmids were introduced into BL21 (DE3) pLys S cells (Promega, Fitchburg, WI, USA), after which the glutathione-S-transferase (GST)-tagged fusion proteins were expressed as described previously.[16]

3-2-5. BLI-ELISA

Bacteria expressing each RLuc-fused FLAP candidate were lysed by freeze-thaw treatment and sonication. After ultracentrifugation at 210,000 × *g* for 15 min, bioluminescence imaging of the supernatant was acquired for 30 s to determine the concentration of sample proteins based on the sample reaction with the RLuc substrate coelenterazine-h (10 ng/μl in PBS; Promega) using an IVIS Lumina *in vivo* imaging system (PerkinElmer, Waltham, MA, USA). Each BLI-ELISA was carried out at room temperature in 96-well black plates. The wells were first coated with HER2-Fc (50 ng/50 μl in PBS; ACRO Biosystems, Newark, DE, USA) overnight, blocked with PBS containing 2% Perfect-Block (MoBiTec, Göttingen, Germany) (PBS-PB) for 2 h, incubated with 100 μl of 1 μM sample proteins for 1 h and washed three times with PBS containing 0.05% Tween-20 (PBS-T). After the addition of coelenterazine-h to each well, bioluminescence imaging was acquired for 30 s.

3-2-6. ELISA

GST-fused and His-tagged FLAPs were purified from the supernatants of bacterial extracts by affinity chromatography using GSTrap HP columns (GE Healthcare) with an AKTA pure 25 system (GE Healthcare). After protease-cleavage by PreScission Protease (GE Healthcare), His-tagged monomeric FLAPs were purified using HisTrap HP columns (GE Healthcare) with an AKTA pure 25 system and dialyzed against PBS. Each ELISA was carried out at room temperature in 96-well black plates. The wells were first coated with HER2-Fc (50 ng/50 μl in PBS) overnight, blocked with 2% PBS-PB for 2 h, incubated with sample proteins in 2% PBS-PB for 1 h and then washed three times with 0.05% PBS-T. After incubation with 1000-fold diluted HRP-conjugated anti-His-tag antibodies (Abcam,

Cambridge, MA, USA) in 2% PBS-PB for 1 h, the wells were washed three times with 0.05% PBS-T and three times with PBS. Fluorescence signals generated by using a QuantaRed Enhanced Chemifluorescent HRP Substrate kit (Thermo Fisher Scientific) were measured by using an Infinite F500 (Tecan, Mannedorf, Switzerland) with specific filters (Ex/Em = 535 nm/590 nm). For the detection of trastuzumab (Chugai Pharmaceutical, Tokyo, Japan) and trastuzumab-Fab (provided by Sysmex Corporation, Kobe, Japan), HRP-conjugated anti-human Kappa light chain (Abcam) and HRP-conjugated anti-human IgG (Fab) (Merck KGaA, Darmstadt, Germany), respectively, were used.

For specificity evaluation, the wells were incubated overnight with HER2-Fc (50 ng/50 μl in PBS), EGFR-Fc (50 ng/50 μl in PBS; R&D systems, MN, USA) or 50 μl PBS and then used as the antigen-coated wells in ELISAs.

For binding competition assays, 100 nM His-tagged monomeric FLAPs mixed with 100 nM trastuzumab in 2% PBS-PB were used as the sample protein in ELISAs.

3-2-7. Biolayer interferometry

The kinetics of FLAP binding to HER2 was studied using a FortéBio Octet Red instrument. The assays were performed at 30 °C in 96-well black plates. HER2-Fc was biotinylated using a biotin labelling kit (Dojindo, Kumamoto, Japan) and 100 nM biotinylated HER2-Fc in the kinetic buffer (0.1% BSA, 0.002% Tween-20 in PBS) was used to load the ligand onto the surface of streptavidin biosensors for 300 s. After washing (30 s) and equilibrating (60 s) the biosensor, the association of the ligand on the biosensor to the analyte in solution (100–1000 nM His-tagged monomeric FLAPs or 1.25–20 nM trastuzumab-Fab) was measured for 300 s. The

dissociation of the interaction was subsequently measured for 300 s. Systematic baseline drift correction was done by subtracting the shift recorded for sensors loaded with ligand but incubated without analyte. Data analysis and curve fitting were done using Octet software version 11.0. Experimental data were fitted with the binding equations available for a 1:1 interaction with local fitting and the mean ± standard error of the mean (SEM) values of k_{on} and k_{off} were calculated from the data of five different concentrations of an analyte. The K_D was calculated as the ratio of k_{off}/k_{on}.

3-2-8. Statistical analysis

Data are presented as means ± SEM and were statistically analyzed with a two-sided Student's *t*-test; *p* values of <0.05 were considered statistically significant.

3-3. Results

3-3-1. Selection of antigen-binding CDR hexapeptides

The results thus far suggested that the structure of the hexapeptide from a mAb CDR can be immobilized when it is grafted at the GA sites in scaffolds. HER2 was selected as a model target for creating FLAPs using our strategy, since this molecule is one of the most important target molecules of breast cancer and, thus, there is an abundance of data describing mAbs against HER2.[17] The eleven (TH1–TH11), seven (TL1–TL7) and nine (PH1–PH9) CDR hexapeptides that may bind to HER2 were selected from the V_H domain of trastuzumab, V_L domain of trastuzumab and V_H domain of pertuzumab, respectively, based on the antigen-contact residues in crystal structures (**Fig. 3-3-1-1**). These hexapeptides were replaced *in silico* with an alanine homo-hexapeptide to calculate the binding energy loss caused by the replacement. The V_L domain of pertuzumab had no HER2-binding CDR hexapeptide. Three (TH3, TH4, TH5) and two (PH5, PH6) CDR hexapeptides from the candidate hexapeptides in trastuzumab and pertuzumab, respectively, showed drastically reduced binding energy following their replacement (**Fig. 3-3-1-1**). The results suggest that these sequences are crucial for maintaining strong interactions with HER2.

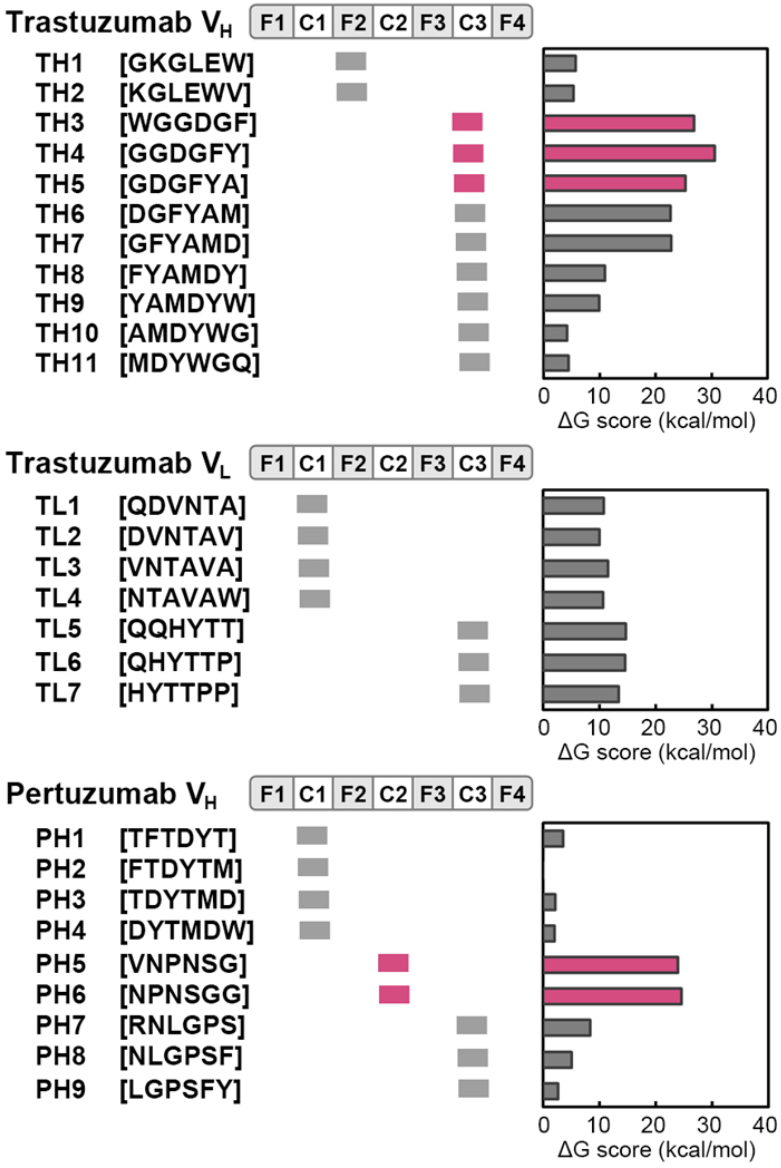

Figure 3-3-1-1. Identification of high-affinity HER2-binding CDR hexapeptides. The names and amino acid sequences of the HER2-binding CDR hexapeptides in the variable domains (V_L and V_H) of trastuzumab and pertuzumab are shown on the left of each panel. F1, C1, F2, C2, F3, C3 and F4 within the upper box in each panel represent the FR1, CDR1, FR2, CDR2, FR3, CDR3 and FR4 domains of the indicated antibodies, respectively. The position of each hexapeptide is shown under the box. The binding energy loss caused by the replacement of each HER2-binding CDR hexapeptide with an alanine homo-hexapeptide is shown in the right graphs. The high-affinity HER2-binding CDR hexapeptides are indicated by magenta coloring.

These five CDR hexapeptides were each grafted into the previously selected 13 GA sites in six scaffolds to generate a total of 65 FLAP candidates: For convenience, the FLAP candidates were named as [Name of GA site]-[Name of grafted CDR hexapeptide] (Sca4-1-TH3–Sca12-1-PH6). As expected, the RMSF values of all grafted CDR hexapeptides were less than 1.5 Å (**Fig. 3-3-1-2a**), confirming that our structural constraint index (1.5 Å) and screening methods are reliable. Since the structure of the immobilized peptide varies depending on the scaffold structure, the root-mean-square deviation (RMSD) values of the CDR hexapeptides in the scaffolds varied from those in their original crystal structures (**Fig. 3-3-1-2b**).

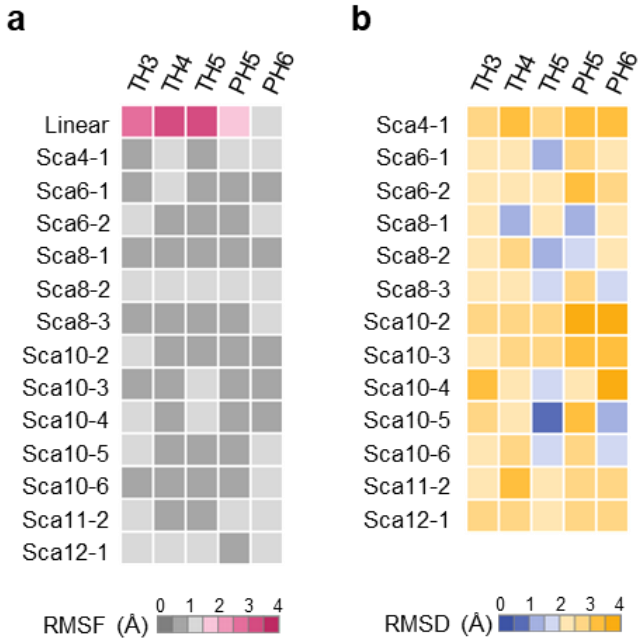

Figure 3-3-1-2. Fluctuation and shape of anti-HER2 FLAP candidates. (a) Structural fluctuation of CDR hexapeptides grafted into scaffolds. The FLAP candidates with an average RMSF value of less or more than 1.5 Å are shown by gray- or magenta-colored squares, respectively. (b) Structural similarity of CDR hexapeptides grafted into scaffolds with corresponding hexapeptides in antibody-HER2 complex structures. RMSD values of less or more than 2.0 Å are shown by blue- or orange-colored squares, respectively.

3-3-2. Rapid identification of antigen-binding FLAPs

The FLAPs with high binding affinity for HER2 were experimentally identified by screening with a fast and easy method using bioluminescence, which is a highly sensitive method to quantitatively analyze target-binding proteins even without protein purification.[18] The FLAP candidates fused with GST and RLuc[19] were expressed as a dimeric form in *Escherichia coli* and the resulting crude extract was used to examine the binding activities of FLAP candidates to HER2 using a BLI-ELISA (**Fig. 3-3-2-1a**). Among the 65 FLAP candidates, strong bioluminescence signals were detected in all the FLAP candidates with Sca8-1 and Sca8-3 GA sites (**Fig. 3-3-2-1b**). In particular, Sca8-1-TH3, Sca8-1-TH5, Sca8-3-TH3 and Sca8-3-TH5 showed very strong bioluminescence signals (**Figs. 3-3-2-1b** and **c**).

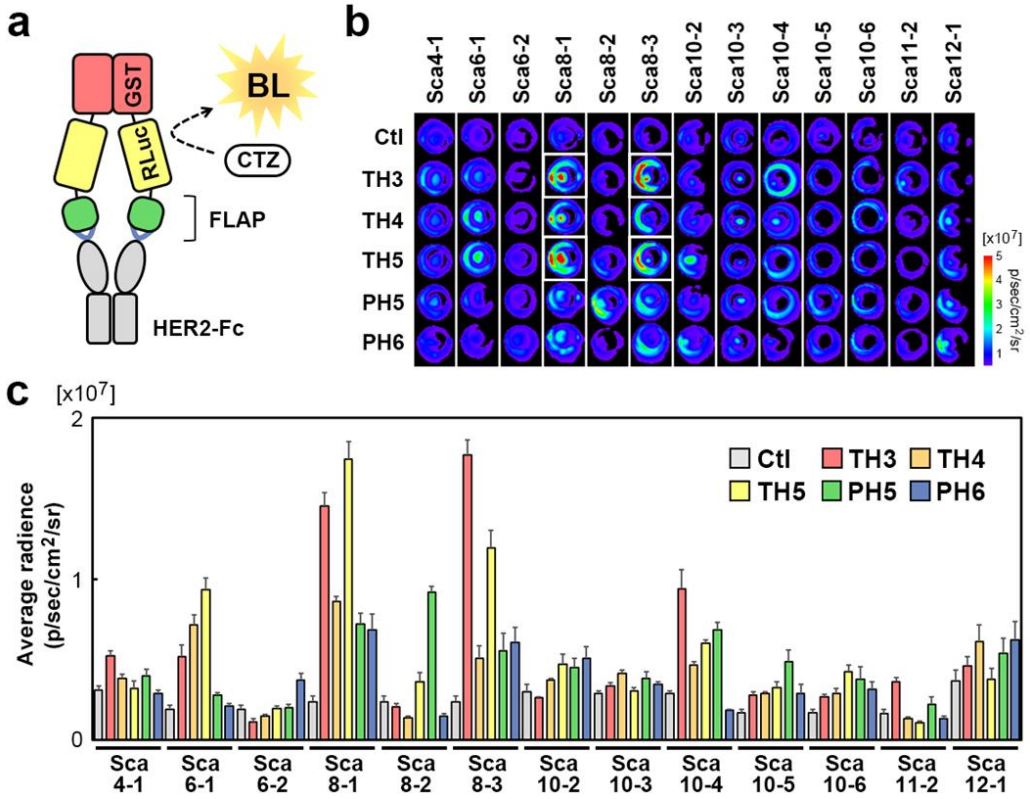

Figure 3-3-2-1. Rapid evaluation of FLAP candidates. (a) Schematic diagram of the RLuc-fused FLAP structure and the principal for affinity determination by BLI-ELISA. The binding affinity of FLAP candidates to HER2-Fc was quantified by the bioluminescence (BL) signal intensity obtained by the reaction between RLuc and coelenterazine (CTZ). (b, c) The HER2-Fc binding activity of the 65 FLAP candidates. FLAP candidates, each consisting of a scaffold (any of Sca4-1 to Sca12-1) and CDR-derived hexapeptide (any one of TH3, TH4, TH5, PH5 or PH6), were evaluated by BLI-ELISA for binding activity to HER2-Fc. Control (Ctl) is the specified RLuc-fused scaffold without a CDR-derived hexapeptide. A representative BL image of the BLI-ELISA plates is shown (b) and the average radiance of each well from three independent experiments is shown as the mean ± SEM (c). White frames in (b) indicate the wells of Sca8-1-TH3, Sca8-1-TH5, Sca8-3-TH3 and Sca8-3-TH5.

The HER2-binding peptide (K_D = 536 nM) were reported to detect HER2 high-expression tumors *in vivo*,[20] suggesting that a moderate affinity is promising for clinical relevance. All candidates showed K_D values between 270 and 550 nM when the FLAP structure of each of these four candidates was purified as a monomeric form and their binding affinity to HER2 was determined by biolayer interferometry (**Fig. 3-3-2-2** and **Table 3-3-2**). These values are about 570–1200 times higher than the K_D value of the parental trastuzumab-Fab (**Table 3-3-2**). In addition, the affinity of these FLAPs in ELISA is 24–65 nM, about 350–960 times higher than that of the parental trastuzumab-Fab, but 150–400 times lower than the K_D values of the peptides fused to the C-terminus of the scaffolds (Sca8-Cterm-TH3 and Sca8-Cterm-TH5), consistent with the previous observations[16] (**Fig. 3-3-2-3** and **Table 3-3-2**). The developed three AbP-FLAPs share same FN3 scaffold (Sca 8), indicating that FN3 is a promising scaffold protein for creation of antibody mimetics.

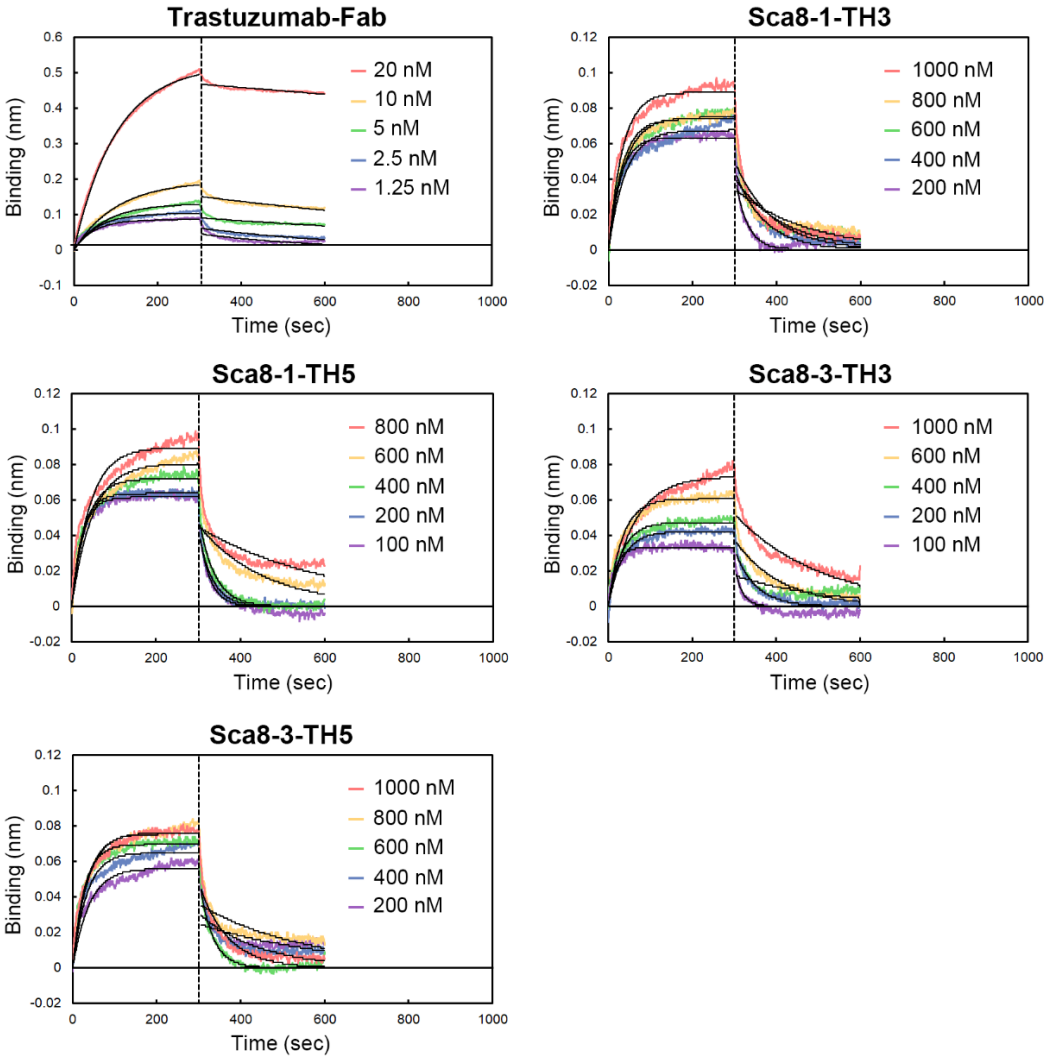

Figure 3-3-2-2. Affinity measurement by biolayer interferometry. Biotinylated HER2-Fc was immobilized on streptavidin biosensors and exposed to various concentrations of trastuzumab-Fab or FLAP candidates. The representative sensorgrams from three experiments were shown.

Table 3-3-2. Affinity toward HER2 of trastuzumab, the Sca8 scaffold and Sca8-based FLAPs

Trastuzumab, scaffold and FLAPs	Biolayer interferometry			ELISA
	K_D (nM)	k_{on} ($10^4 M^{-1}s^{-1}$)	k_{off} ($10^{-2}s^{-1}$)	K_D (nM)
Trastuzumab (divalent)	ND[a]	ND	ND	0.015 ± 0.0032
Trastuzumab-Fab	0.47	290 ± 30	0.14 ± 0.015	0.068 ± 0.014
Sca8-Ctl	ND	ND	ND	>10000
Sca8-Cterm-TH3	ND	ND	ND	>10000
Sca8-Cterm-TH5	ND	ND	ND	>10000
Sca8-1-TH3	350	2.6 ± 0.12	0.90 ± 0.077	64 ± 10
Sca8-1-TH5	270	3.9 ± 0.29	1.1 ± 0.27	24 ± 3.2
Sca8-3-TH3	330	2.7 ± 0.30	0.87 ± 0.14	65 ± 8.1
Sca8-3-TH5	550	2.6 ± 0.49	1.4 ± 0.022	52 ± 14
Sca8-2-TH5	ND	ND	ND	860 ± 45

[a] ND, Not determined

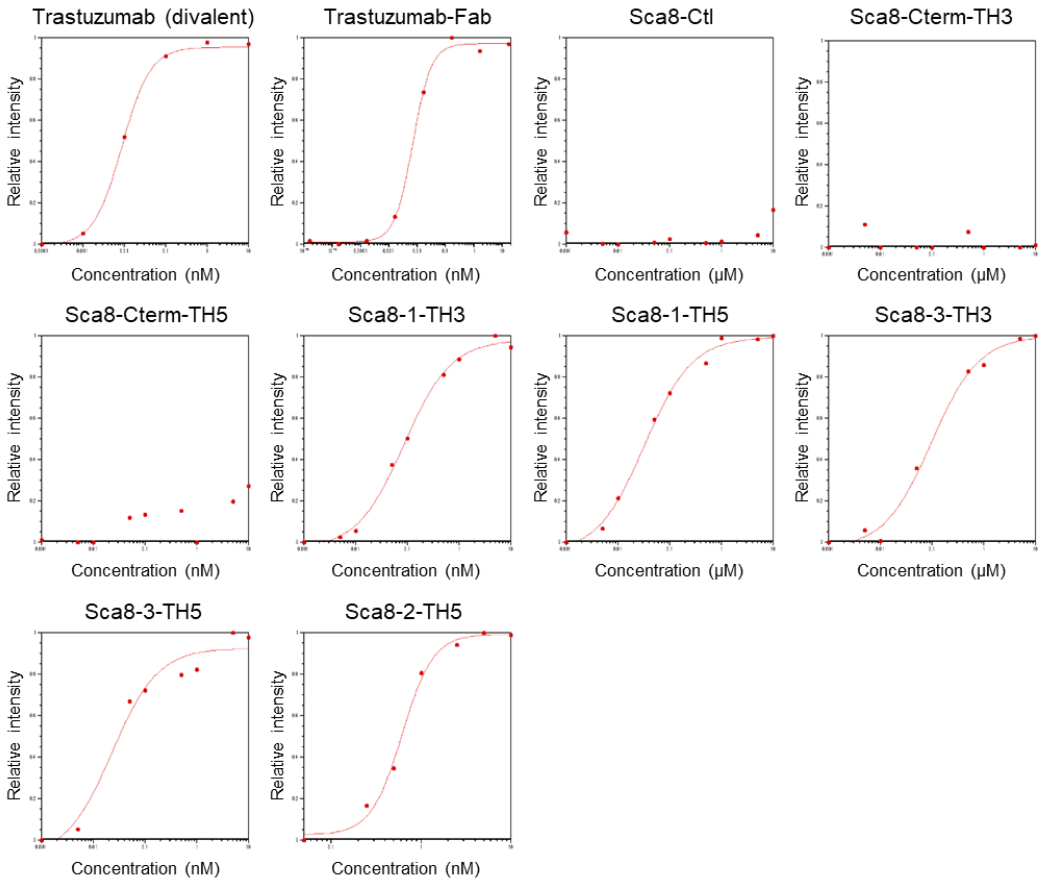

Figure 3-3-2-3. Affinity measurement by ELISA. HER2-Fc was immobilized on ELISA plates and exposed to various concentrations of trastuzumab, trastuzumab-Fab, Sca8-Ctl or FLAP candidates. Binding was detected with an anti-human Kappa light chain-HRP antibody for trastuzumab, an anti-human IgG (Fab)-HRP antibody for trastuzumab-Fab or an anti-His tag-HRP antibody for Sca8 and FLAP candidates. The results are representative of three experiments.

3-3-3. Characterization of the anti-HER2 FLAPs

The four AbP-FLAP candidates were examined for their binding specificity as alternatives to the primary antibody. When the affinities of these FLAPs to HER2-Fc, epidermal EGFR-Fc or non-coated wells were evaluated by ELISA, the FLAPs specifically bound to HER2-Fc and hardly bound to EGFR-Fc and non-coated wells (**Fig. 3-3-3a**). As they all share their target binding sequences with trastuzumab, competitive binding was examined by incubating these FLAPs with HER2-Fc

proteins in the presence of trastuzumab. The binding amount of three AbP-FLAPs, Sca8-1-TH3, Sca8-1-TH5 and Sca8-3-TH3, decreased significantly in the presence of trastuzumab (**Fig. 3-3-3b**), confirming that the FLAPs bind to the same epitope as trastuzumab. In contrast, Sca8-3-TH5 was suggested to bind to HER2-Fc with the different epitope from trastuzumab (**Figs. 3-3-3a** and **b**). Therefore, we hereinafter regard these three candidates, Sca8-1-TH3, Sca8-1-TH5 and Sca8-3-TH3, as AbP-FLAP 1, AbP-FLAP 2 and AbP-FLAP 3, respectively. These results indicate that the AbP- FLAPs have high specificity toward HER2.

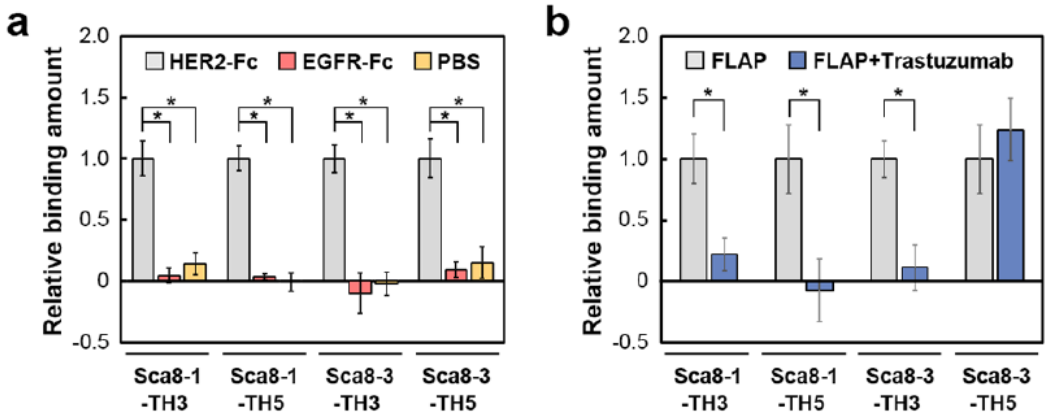

Figure 3-3-3. Characterization of AbP-FLAPs. (a) Specific binding of AbP-FLAP candidates to HER2. FLAP candidates binding to HER2-Fc, EGFR-Fc or non-coated well (PBS) were evaluated by ELISA. The mean ± SEM of three independent experiments is shown; *$p < 0.05$. (b) Binding competition between AbP-FLAP candidates and their parental mAb. His-tagged FLAPs (100 nM) were mixed with 100 nM trastuzumab or buffer and FLAP candidates binding to HER2-Fc were evaluated by ELISA. The mean ± SEM of three independent experiments is shown; *$p < 0.05$.

Discussion

This study clearly demonstrated that the strategy of grafting the immobilized AbPs into the appropriate scaffolds is a reliable method for generating high-performance antibody mimetics that bind to the same epitopes as the mAbs from which the AbPs are derived. The proposed design strategy successfully developed an immobilized AbP-grafted non-Ig affinity protein, FLAP, which demonstrated efficient binding to HER2. In addition, the FLAPs were found to barely bind to EGFR, which belongs to the same receptor family as HER2, indicating that the mAb specificity of the target-binding peptides is also retained in the FLAPs. The FLAP property that the molecular size is small enough for chemical synthesis and the epitope is identical to the parental antibody is a key advantage of FLAPs over fragment antibodies, which are relatively large molecules. This design strategy for developing AbP-FLAPs can be applied to many mAbs, facilitating the development of alternatives to antibodies already used in clinical and basic research.

Amino acid sequences of antibody CDRs would be optimized during the affinity maturation process to decrease the entropic cost on antigen binding and to increase the enthalpic contribution.[21–24] A computational prediction provides specific indicators for structural immobilization. It also revealed that almost all CDRs are immobilized in antibody FRs (Fig. 2-3-2-3) and that FRs retain a high capacity to reduce the fluctuation of various peptides (Fig. 2-3-3-1), clearly showing that FRs function as a general scaffold to reduce the entropic energy loss of CDRs on antigen binding. Furthermore, CDR-derived short peptides often lose their antigen-affinity when released from FRs. Ideally, the CDR-derived short peptides in FLAPs would be expected to have high affinity, similar to that of the parental antibodies, because they are structurally immobilized in essentially the

same structure as antibody FRs. However, our method developed only three FLAPs out of 65 anti-HER2 FLAP candidates, indicating that the CDR peptides in most FLAP candidates are not optimally immobilized. The anti-HER2 FLAP candidates were immobilized (Fig. 3-3-2-2a) with various structures (Fig. 3-3-2-2b) and various affinities against HER2 (Fig. 3-3-3-1 and Table 3-3-3), confirming that an appropriate CDR hexapeptide structure is also required for enthalpic interaction. Further optimization of the immobilized structure of pertuzumab-derived CDR hexapeptides in more suitable scaffolds may facilitate the development of high-affinity FLAPs with these hexapeptides. Although a highly accurate structure prediction is needed to validate the accurate enthalpy and entropy changes on antigen binding, the currently applied computational calculation has several limitations, such as the lack of a suitable general algorithm and its high computational complexity. Thus, the semi-rational strategy presented here is one of the most feasible methods for efficiently developing antibody mimetics.

The AbP-FLAPs were successfully designed with the new method but the affinities of these FLAPs were still lower than those of the parent antibodies. A possible engineering strategy to increase the affinity of FLAPs involves multiple grafting of immobilized CDR-derived peptides. The strategy may be successful because antibody paratopes are often formed by a combination of dominant CDRs and ancillary CDRs. In the case of trastuzumab, for example, CDR-H3 is the dominant CDR, and CDR-L1 and CDR-L3 are the ancillary CDRs. In this study, each FLAP has only one CDR hexapeptide from CDR-H3. The additional grafting of CDR hexapeptides from CDR-L1 and CDR-L3 onto the FLAPs with favorable geometry may improve the affinity of these FLAPs. Scaffolds such as Sca10 have multiple geometrically proximal GA sites (Table 2-3-2) and thus may be suitable

for grafting multiple CDR-derived peptides to yield higher affinity FLAPs and biparatopic FLAPs.

The dissociation constant (K_D) is determined by the ratio of dissociation (k_{off}) and association (k_{on}) rate constants. Several molecular properties affect the k_{on} and k_{off} values including binding site accessibility, molecular size, hydrophobicity, conformational fluctuations and electrostatic interaction between binders and targets.[25] In the case of AbP-FLAPs, their small molecular size may cause much lower k_{on} values compared to the trastuzumab-Fab, because other small protein binders such as monobodies and nanobodies often have lower k_{on} values than mAbs.[26,27] Therefore, it seems difficult to improve the k_{on} values of AbP-FLAPs to be comparable to mAb. To obtain higher affinity FLAPs, the improvement of k_{off} values by some modifications stabilizing the complex structures of HER2 and FLAPs may be promising way.

Notably, HER2 is expressed at low levels in a wide variety of vitally important normal tissues and thus there is a concern about side effects in HER2-targeting therapies using mAbs.[28] Base on the recent study using a bivalent anti-HER2 engineered antibody,[29] the moderate affinity (K_D) of FLAPs created in this study is within a clinically relevant range, suggesting that mono and multivalent anti-HER2 FLAPs are promising options for developing specific drugs against HER2-amplified cancers. The HER2-binding affibodies or peptides were reported to detect HER2 high-expression tumors *in vivo*.[20,30–32] Their affinity (K_D) toward recombinant HER2 proteins were the range of 22 pM–536 nM, indicating that FLAPs have enough affinity for the development of tumor imaging probes.

Sca8-3-TH5 showed similar affinity and specificity to HER2 with three FLAPs, but its epitope seemed to be different from trastuzumab, suggesting that

novel epitope-binding surface was constructed by the grafting of the AbP, TH5. Although further analysis is required to clarify binding mode of Sca8-3-TH5, this unexpected result would indicate the usefulness of our method to develop a practical antibody mimetics with different paratope from parental mAb.

This study demonstrates the general concept for designing high-performance antibody mimetics by grafting immobilized antigen-binding peptides into non-Ig scaffolds. This strategy is applicable to the generation of antibody mimetics and other functional proteins, including receptor ligands, cytokines, inhibitors and enzymes. Therefore, this study may open new avenues for developing novel technology platforms in protein engineering and biopharmaceutical design. In addition, the identified three AbP-FLAPs has same FN3-based scaffold, indicating that FN3 is a promising scaffold protein for creation of antibody mimetics.

References

1. Raibaut, L., El Mahdi, O. & Melnyk, O. Solid Phase Protein Chemical Synthesis. *Top. Curr. Chem.* **363**, 103–154 (2015).
2. Friedman, M. *et al.* Phage display selection of Affibody molecules with specific binding to the extracellular domain of the epidermal growth factor receptor. *Protein Eng. Des. Sel.* **20**, 189–199 (2007).
3. Löfblom, J., Frejd, F. Y. & Ståhl, S. Non-immunoglobulin based protein scaffolds. *Curr. Opin. Biotechnol.* **22**, 843–848 (2011).
4. Ramamurthy, V. *et al.* Structures of adnectin/protein complexes reveal an expanded binding footprint. *Structure* **20**, 259–269 (2012).
5. Škrlec, K., Štrukelj, B. & Berlec, A. Non-immunoglobulin scaffolds: A focus on their targets. *Trends Biotechnol.* **33**, 408–418 (2015).
6. Weidle, U. H., Auer, J., Brinkmann, U., Georges, G. & Tiefenthaler, G. The emerging role of new protein scaffold-based agents for treatment of cancer. *Cancer Genomics and Proteomics* **10**, 155–168 (2013).
7. Zahnd, C. *et al.* A Designed Ankyrin Repeat Protein Evolved to Picomolar Affinity to Her2. *J. Mol. Biol.* **369**, 1015–1028 (2007).
8. Richards, D. A. Exploring alternative antibody scaffolds: Antibody fragments and antibody mimics for targeted drug delivery. *Drug Discov. Today Technol.* **30**, 35–46 (2018).
9. Chevalier, A. *et al.* Massively parallel de novo protein design for targeted therapeutics. *Nature* **550**, 74–79 (2017).
10. Jones, P. T., Dear, P. H., Foote, J., Neuberger, M. S. & Winter, G. Replacing the complementarity-determining regions in a human antibody with those from a mouse. *Nature* **321**, 522–525 (1986).

11. Almagro, J. C. & Fransson, J. Humanization of antibodies. *Front. Biosci.* **13**, 1619–1633 (2008).

12. Nicaise, M., Valerio-Lepiniec, M., Minard, P. & Desmadril, M. Affinity transfer by CDR grafting on a nonimmunoglobulin scaffold. *Protein Sci.* **13**, 1882–1891 (2004).

13. Inoue, H. *et al.* Affinity transfer to a human protein by CDR3 grafting of camelid VHH. *Protein Sci.* **20**, 1971–1981 (2011).

14. Pacheco, S. *et al.* Affinity transfer to the archaeal extremophilic Sac7d protein by insertion of a CDR. *Protein Eng. Des. Sel.* **27**, 431–438 (2014).

15. Case, D. A. *et al. Amber 2017*. *University of California, San Francisco* (2017). doi:citeulike-article-id:2734527

16. Kadonosono, T. *et al.* A fluorescent protein scaffold for presenting structurally constrained peptides provides an effective screening system to identify high affinity target-binding peptides. *PLoS One* **9**, e103397 (2014).

17. Larionov, A. A. Current therapies for human epidermal growth factor receptor 2-positive metastatic breast cancer patients. *Front. Oncol.* **8**, 89 (2018).

18. Kadonosono, T. *et al.* Domain architecture of vasohibins required for their chaperone-dependent unconventional extracellular release. *Protein Sci.* **26**, 452–463 (2017).

19. Loening, A. M., Dragulescu-andrasi, A. & Gambhir, S. S. A red-shifted Renilla luciferase for transient reporter-gene expression. *Nat. Methods* **7**, 5–6 (2010).

20. Yang, X. *et al.* Peptide probes derived from pertuzumab by molecular dynamics modeling for HER2 positive tumor imaging. *PLoS Comput. Biol.*

13, e1005441 (2017).

21. Babor, M. & Kortemme, T. Multi-constraint computational design suggests that native sequences of germline antibody H3 loops are nearly optimal for conformational flexibility. *Proteins Struct. Funct. Bioinforma.* **75**, 846–858 (2009).

22. Manivel, V., Sahoo, N. C., Salunke, D. M. & Rao, K. V. S. Maturation of an antibody response is governed by modulations in flexibility of the antigen-combining site. *Immunity* **13**, 611–620 (2000).

23. Thorpe, I. F. & Brooks, C. L. Molecular evolution of affinity and flexibility in the immune system. *Proc. Natl. Acad. Sci. U. S. A.* **104**, 8821–8826 (2007).

24. Wong, S. E., Sellers, B. D. & Jacobson, M. P. Effects of somatic mutations on CDR loop flexibility during affinity maturation. *Proteins Struct. Funct. Bioinforma.* **79**, 821–829 (2011).

25. Pan, A. C., Borhani, D. W., Dror, R. O. & Shaw, D. E. Molecular determinants of drug-receptor binding kinetics. *Drug Discov. Today* **18**, 667–673 (2013).

26. Duan, J., Wu, J., Valencia, C. A. & Liu, R. Fibronectin type III domain based monobody with high avidity. *Biochemistry* **46**, 12656–12664 (2007).

27. Hussack, G., Raphael, S., Lowden, M. J. & Henry, K. A. Isolation and characterization of camelid single-domain antibodies against HER2. *BMC Res. Notes* **11**, 866 (2018).

28. Junttila, T. T. *et al.* Antitumor efficacy of a bispecific antibody that targets HER2 and activates T cells. *Cancer Res.* **74**, 5561–5571 (2014).

29. Slaga, D. *et al.* Avidity-based binding to HER2 results in selective killing of HER2-overexpressing cells by anti-HER2/CD3. *Sci. Transl. Med.* **10**,

eaat5775 (2018).

30. Orlova, A. *et al.* Tumor imaging using a picomolar affinity HER2 binding Affibody molecule. *Cancer Res.* **66**, 4339–4348 (2006).

31. Kumar, S. R., Quinn, T. P. & Deutscher, S. L. Evaluation of an 111in-radiolabeled peptide as a targeting and imaging agent for ErbB-2 receptor-expressing breast carcinomas. *Clin. Cancer Res.* **13**, 6070–6079 (2007).

32. Geng, L. *et al.* HER2 targeting peptides screening and applications in tumor imaging and drug delivery. *Theranostics* **6**, 1261–1273 (2016).

Chapter 4

Development of FLAPs by grafting HBPs

Abstract

Tumor-binding peptides such as HER2-binding peptides (HBPs) are attractive therapeutic and diagnostic options for cancer. However, the HBPs developed thus far are susceptible to proteolysis and lose their affinity to HER2 *in vivo*. This chapter describes a method to create a HER2-binding fluctuation-regulated affinity protein (HBP-FLAP) consisting of a structurally immobilized HBP and a FN3, which is the most appropriate scaffold for HBP grafting as described in Chapter 3. In this method, HBP was first selected by phage-library screening, grafted into FN3, then improved the binding affinity by affinity maturation. HBP-FLAP containing YCAHNM peptide shows increased proteolysis-resistance, specifically binding to HER2 with a K_D of 58 nM in ELISA and 287 nM in biolayer interferometry. The proteolytic resistance of HBP was improved in HBP-FLAP. Consequently, I concluded that FN3-based FLAP is an excellent platform for developing target-binding small proteins.

4-1. Introduction

4.1.1 Target-binding peptides

Tumor-binding peptides are a promising alternative to mAbs as they demonstrate greater tumor penetration because of their small molecular size.[1] Various kinds of HBPs have been identified, including a linear peptide KCCYSL,[2] bicyclic peptides ACYLQDPNCDWWGPYCGGSG[3] and a trastuzumab-derived cyclic peptide FCGDGFYACYMDV.[4] Trastuzumab- and pertuzumab-derived peptides, QDVNTAVAW and EWVADVNPNSGGFIYNQYFK, respectively, have also been designed and used in tumor imaging.[5,6] However, their clinical application is limited to use as diagnosis probes because short peptides are very sensitive to protease activity in circulation and tissues, resulting in reduced binding to targets. Therefore, proteins with proteolysis-resistant target-binding peptides may increase the applicability of tumor-binding peptides for clinical use.

4-1-2. Use of FN3 as a small protein scaffold

The FN3, one of three types of internal repeats found in the plasma protein fibronectin, was selected as a scaffold because computational calculations in chapter 2 revealed that the FN3 has three GA sites in which the structure of grafted hexapeptides can be immobilized. FN3 is an endogenous protein with small molecular size (10 kDa), high stability and high solubility.[7,8] FN3 has been already used for the development of affinity proteins targeting various antigens by protein engineering,[8,9] some of which have already been in clinical trials,[10] suggesting that FN3 is a promising scaffold protein for creating HBP-FLAPs.

In this chapter, HBPs were screened by phage display technique and were grafted into FN3 scaffold to generate FN3-HBP candidates. The binding affinity of

one FN3-HBP was then improved by affinity maturation. Finally, HBP-FLAP with highest binding affinity among candidates was identified.

4-2. Materials and Methods

4-2-1. Peptide screening

The T7 phage libraries displaying the random cyclic peptides $X_3CX_8CX_3$ or $X_3CX_9CX_3$, where X represents the randomized amino acids, were constructed using the T7 Select10-3b vector (Merck Millipore, MA, USA), as described previously.[11] HER2-Fc protein (R&D systems, CA, USA) was biotinylated using labeling kit (Dojindo, Kumamoto, Japan) and immobilized on streptavidin-conjugated magnetic beads (Tamagawa seiki, Nagano, Japan). The beads were blocked with 0.5% BSA in PBS, incubated with the phage libraries of $X_3CX_8CX_3$ (1×10^{10} pfu) or $X_3CX_9CX_3$ (1×10^{10} pfu) for 1 h, washed 30 times with PBS with 1% Tween 20 (1% PBST) and then added to 7 mL of *E. coli* BLT5403 cells (Merck Millipore) in log phase growth. After incubation at 37 ºC and bacteriolysis, the phages were recovered from the culture supernatant by centrifugation (9,100 g for 10 min at 4 °C) and used for the next round of biopanning. Amino acid sequences of displayed cyclic peptides on selected T7 phage clones were analyzed by DNA sequencing.

4-2-2. ELISA

For phage-ELISA, the wells of a 96-well black plates (Thermo Fisher Scientific, MA, USA) were coated with 1,000 ng of HER2-Fc, streptavidin (Wako, Osaka, Japan) or IgG1-Fc (R&D systems) and blocked with 2% Perfect-Block (MoBiTec, Göttingen, Germany) in PBS for 1 h. Phage solution (1×10^{10} pfu) were added to each well and incubated for 1 h. After washing the plate, the bound phages were detected with anti-T7 fiber tail antibody (Merck Millipore) as a primary antibody and anti-mouse IgG HRP-linked antibody (Cell Signaling Technology,

Danvers, MA).

For indirect ELISA, the wells were first coated with 50 ng of HER2-Fc, blocked with 2% Perfect-Block in PBS for 2 h. After incubation with sample proteins for 1 h, HRP-conjugated anti-His-tag antibody (Abcam, Cambridge, MA, USA) was incubated for 1 h with the samples and then treated with QuantaRed Enhanced Chemifluorescent HRP Substrate kit (Thermo Fisher Scientific). The resulting fluorescence was measured using an Infinite F500 (Tecan, Mannedorf, Switzerland) with specific filters (Ex/Em = 535 nm/590 nm).

For specificity evaluation, the wells were incubated overnight with HER2-Fc (50 ng/50 μL in PBS), EGFR-Fc (50 ng/50 μL in PBS; R&D systems) or 50 μL PBS and applied to the indirect ELISA described above.

4-2-3. MD simulation

Initial coordinates of the FN3 protein were taken from the Protein Data Bank (PDB ID: 1TTG). The structures of linear peptides and FN3 mutants were generated using Discovery studio 3.1 (Accelrys, San Diego, CA, USA). The systems were optimized via energy minimization and equilibrated with backbone restraints. Production runs were performed for at least 10 ns for trajectory analysis. All MD simulations were performed using the Amber 14 and 16 program packages[12] on TSUBAME (Global Scientific Information Center, Tokyo Institute of Technology). The Amber ff14SB force fields and the GB/SA implicit solvent model were used. The time-step for MD simulations was set to 2 fs with the SHAKE algorithm. A nonbonded cutoff of 999.9 Å was used. The temperature was kept constant at 300 K using the Berendsen rescaling method. The RMSF of all hydrogen-free atoms during the final 5 ns of each production run were calculated to investigate the

backbone fluctuations in each system using the cpptraj module.

4-2-4. Plasmid construction and protein purification

The recombinant DNA experiment was carried out according to the necessary regulations based on the Tokyo Institute of Technology recombinant DNA experimental safety management regulations defined by the Tokyo Institute of Technology recombinant DNA experimental safety management committee. The cDNA encoding the fusion protein, consisting of His-tag, GGGS linker and FN3 (H-FN3), was inserted into the multi-cloning site of pGEX-6P-3 plasmid (GE Healthcare, Little Chalfont, UK). The plasmid vectors expressing H-FN3 and H-FN3 mutants were transformed into *E. coli* BL21 (DE3) pLysS cells (Promega, Fitchburg, WI, USA). These proteins were expressed in the bacteria as GST fused proteins. GST-fused H-FN3 and H-FN3 mutants were purified from the supernatants of bacterial extracts using glutathione agarose (Sigma-Aldrich, MO, USA). After protease-cleavage of GST by PreScission Protease (GE Healthcare), the monomeric proteins were purified again using HisTrap HP columns (GE Healthcare), according to the manufacturer's instructions, to increase protein sample purity.

4-2-5. Biolayer Interferometry

The kinetics of HBP-FLAP binding to HER2 was studied using a ForteBio Octet Red (ForteBio, CA, USA) instrument. The assays were performed at 30 °C in 96-well black plates. HER2-Fc was biotinylated using a biotin labelling kit (Dojindo) and 100 nM biotinylated HER2-Fc in the kinetic buffer (0.1% BSA, 0.002% Tween-20 in PBS) was used to load the ligand onto the surface of

streptavidin biosensors (ForteBio) for 300 s. After washing (30 s) and equilibrating (60 s) the biosensor, the association of the ligand on the biosensor to the analyte in solution (100–800 nM His-tagged HBP-FLAP in the kinetic buffer) was measured for 300 s. The dissociation of the interaction was subsequently measured for 300 s. Systematic baseline drift correction was done by subtracting the shift recorded for sensors loaded with ligand but incubated without analyte. Data analysis and curve fitting were done using Octet software version 11.0 (ForteBio). Experimental data were fitted with the binding equations available for a 1:1 interaction with local fitting and the mean ± SEM values of k_{on} and k_{off} were calculated from the data of four different concentrations of analytes. The K_D was calculated as the ratio of k_{off}/k_{on}.

4-2-6. Proteinase K treatment

Fifty μM of FN3-p1.M.2 or the C-terminally elongated p1.M.2 peptide (YCAHNM-GSGSGK) was digested by 50 μU/mL proteinase K for 2 h in 10 mM Tris-HCl (pH 8.0) containing 10 mM EDTA. Sample aliquots were collected at various reaction times and analyzed by SDS-PAGE or reversed-phase high-performance liquid chromatography (HPLC; InsertSustainSwift C18 column; GL Sciences, Tokyo, Japan). The ratio of intact FN3-p1.M.2 and the C-terminally elongated p1.M.2 peptide were calculated based on the band intensity of the digested products on the SDS-PAGE gel and the HPLC peaks in the chromatogram, respectively.

4-2-7. Statistical analysis

Data in this study are expressed as means ± SEM. Differences are analyzed

with a two-sided Student's *t*-test; *p* values of <0.05 were considered as statistically significant.

4-3. Results

4-3-1. Strategy for creating HBP-FLAP

Our previous research demonstrated that short peptides grafted in a particular region of protein scaffold were structurally immobilized and showed increased resistance to protease.[13] This finding prompted us to develop clinically applicable HER2-binding small proteins with a structurally immobilized HBP. **Fig. 4-3-1** shows a process for producing such protein HBP-FLAP.

The HBPs were first isolated from a phage-displayed peptide library (**Fig. 4-3-1A**) and then some six consecutive amino acids (hexapeptides) in the isolated HBPs were selected and were grafted into the GA site of FN3 to create FN3-HBPs (**Fig. 4-3-1B**). The binding affinity of the FN3-HBPs was improved by affinity maturation (**Fig. 4-3-1C**). The affinity-matured HBP-FLAP that showed the highest binding affinity among the tested FN3-HBPs was labeled with the near-infrared fluorescence dye IRDye 800CW which is used in chapter 5 to investigate a target-binding *in vivo* (**Fig. 4-3-1D**).

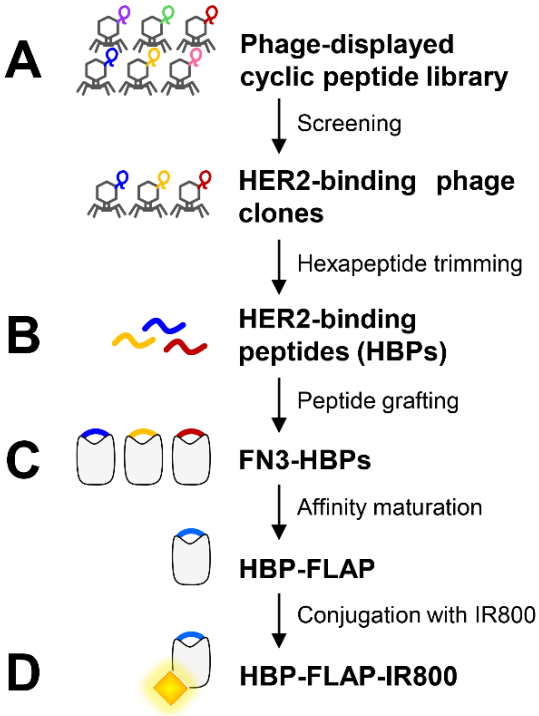

Figure 4-3-1. Overview of HBP-FLAP development by grafting HBP into small protein scaffold for peptide stabilization. (A) The HBPs were isolated from phage-displayed cyclic peptide library. (B) Hexapeptides trimmed from HBPs were grafted into the GA site of FN3 scaffold to generate FN3-HBPs. (C) Binding affinity of FN3-HBP was improved by affinity maturation using alanine scanning and the FN3-HBP with the highest affinity was screened using phage-displayed FN3-HBP mutant library to create the optimal HBP-FLAP. (D) The affinity-matured HBP-FLAP was conjugated with near infrared fluorescence dye IRDye 800CW (IR800) to give an *in vivo* imaging probe, HBP-FLAP-IR800.

4-3-2. Design of a HER2-binding small proteins

Five T7 phage clones, P1–P5, displaying HBPs were enriched by eight rounds of biopanning against HER2-Fc from T7 phage libraries displaying random cyclic peptides $X_3CX_8CX_3$ or $X_3CX_9CX_3$, where X represents the randomized amino acids (**Fig. 4-3-2A**). Further evaluation of the phage clones by phage-ELISA revealed their target specificity: P1, P4 and P5 bind strongly and specifically, whereas P2 binds weakly to HER2-Fc. P3 binds to IgG-Fc non-specifically (**Fig. 4-3-2B**). Therefore, HBPs expressed in P1, P4 and P5 (hereafter named p1, p4 and p5) were used for the development of FN3-HBPs. Continuous hexapeptides p4.1–p4.4 and p5.1–p5.4 were prepared from p4 and p5, respectively (**Table 4-3-2**) and grafted into the GA site of FN3 (**Fig. 4-3-2C**). Note that the p1 was originally displayed as a hexapeptide on T7 phage because the seventh codon is a stop codon. Computational evaluation by MD simulations confirmed a decrease in the average RMSF value. This indicates that all linear hexapeptides were immobilized in the GA site of FN3 (**Fig. 4-3-2D**). As a result, I obtained nine FN3-HBPs: FN3-p1, FN3-p4.1, FN3-p4.2, FN3-p4.3, FN3-p4.4, FN3-p5.1, FN3-p5.2, FN3-p5.3 and FN3-p5.4.

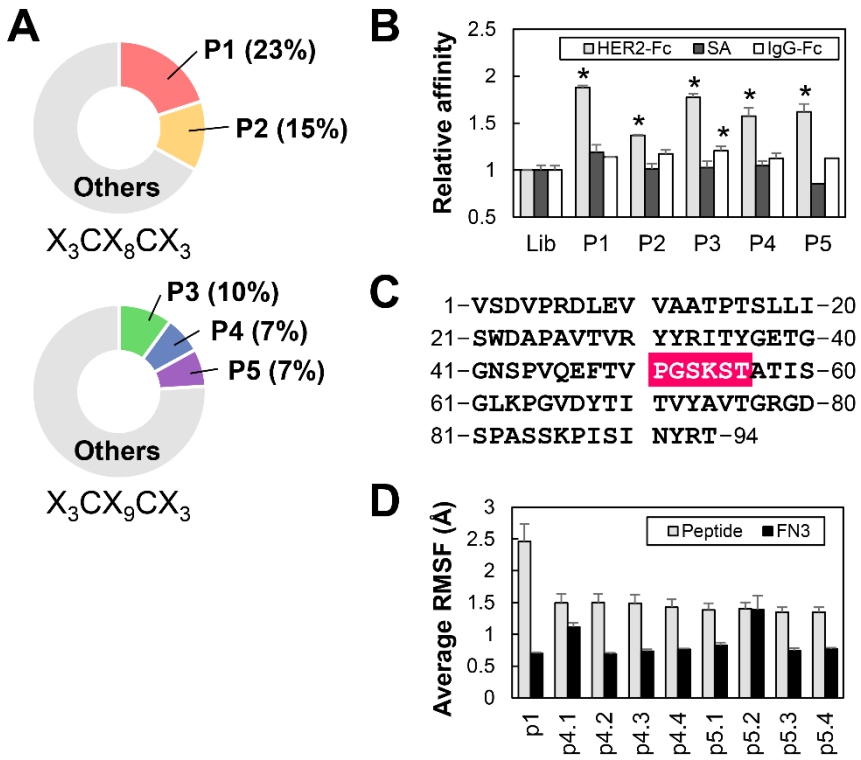

Figure 4-3-2. Preparation of HBP-FN3s. (A) The frequency of detection of HBPs during the phage library screening. Phage clones P1 and P2 were selected from an eight-amino acid cyclic peptide ($X_3CX_8CX_3$) library. Phage clones P3–P5 were selected from a nine-amino acid peptide ($X_3CX_8CX_3$) library. (B) The binding affinity of the indicated phage clones to HER2-Fc (grey), streptavidin (SA, black) and IgG-Fc (white) were measured by ELISA and the relative affinities to the control cyclic peptide library (Lib) are shown. $n = 3$, mean ± S.E.M., $*p < 0.05$ compared with Lib based on a Student's *t*-test. (C) Amino acid sequence of the FN3 domain. The HBP was grafted into FN3 by substitution at residues 51–56, which are highlighted in pink. (D) RMSF calculation of HBPs in linear form (grey) and grafted into the FN3 scaffold (black).

Table 4-3-2. Amino acid sequences of the HER2-binding peptides

Peptides	Amino acid sequences
p1	YCGCEM
p2	PFICCRRPRGRRCEHG
p3	SLFCWVRVM
p4	AMVCTRARKPKSGCRRVG
p5	VELCATAKHEVKSCLSFG
p4.1	TRARKP
p4.2	RARKPK
p4.3	ARKPKS
p4.4	RKPKSG
p5.1	ATAKHE
p5.2	TAKHEV
p5.3	AKHEVK
p5.4	KHEVKS

4-3-3. Affinity maturation of HER2-binding small proteins

Recombinant FN3-HBPs were purified by a bacterial protein expression system and used to determine the FN3-HBP with highest affinity to HER2. Two out of the nine FN3-HBPs, FN3-p4.1 and FN3-p5.2, were not expressed but the other seven FN3-HBPs were expressed successfully as soluble proteins and easily purified. Evaluation of the binding affinity to HER2 revealed that three out of the seven, FN3-p1, FN3-p4.3 and FN3-p4.4 bound to HER2 (**Fig. 4-3-3-1A**) with dissociation constants (K_D) 280–500 nM (**Fig. 4-3-3-2A** and **Table 4-3-3-1**), indicating moderate binding affinity. Sequence optimization of p1 with the lowest

K_D value (K_D = 280 nM) was performed to increase the affinity of FN3-p1. By single amino acid substitutions in p1 (YCGCEM) to alanine (A), six FN3-p1 mutants, FN3-p1.1A, FN3-p1.2A, FN3-p1.3A, FN3-p1.4A, FN3-p1.5A and FN3-p1.6A were generated (**Table 4-3-3-2**). Reduced binding affinity to HER2 was observed with FN3-p1.1A, FN3-p1.2A and FN3-p1.6A (**Fig. 4-3-3-1B**), indicating that the first (Y51), second (C52) and sixth (M56) residues were important for HER2 binding. Optimization of the third, fourth and fifth residues of P1 was performed using a T7 phage-displayed FN3-p1 mutant library with three randomized sequences 51-YCXXXM-56. After eight rounds of biopanning, three peptides were selected from the most frequently enriched FN3-p1 mutants: FN3-p1.M.1 (YCICCM), FN3-p1.M.2 (YCAHNM) and FN3-p1.M.3 (YCPVCM; **Fig. 4-3-3-1C** and **Table 4-3-3-2**). Amino acid substitutions made in the third, fourth and fifth residue positions showed minimal effect on structural fluctuations of Y51, C52 and M56 (**Fig. 4-3-3-1D** and **E**). Among the three affinity-matured FN3-p1 mutants, FN3-p1.M.2 showed the highest binding affinity toward HER2 (K_D = 58 nM in ELISA and K_D = 287 nM in biolayer interferometry; **Fig. 4-3-3-2B** and **Table 4-3-3-1**) and was selected for further characterization.

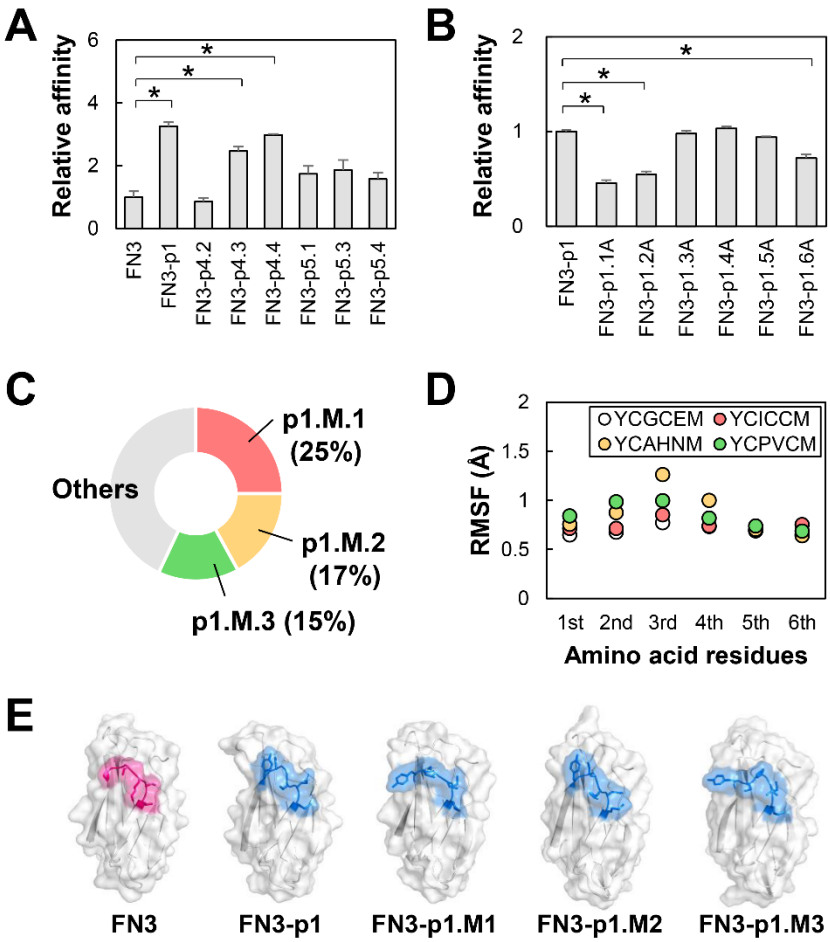

Figure 4-3-3-1. Affinity maturation of HER2-binding small proteins. (A) ELISA was used to measure the affinity of FN3-HBP mutants toward HER2-Fc. The mean ± SEM of three independent experiments is shown; *$p < 0.05$. (B) ELISA measurements showing the affinity of alanine substitution mutants of FN3-p1 toward HER2-Fc. The mean ± SEM of three independent experiments is shown; *$p < 0.05$. (C) The pie chart shows the frequency of detection of the HBP sequence (YCXXXM) in screening after affinity maturation. (D) Fluctuation of the residues of the indicated HBP sequences (YCXXXM) in FN3-p1. The RMSF values of each residue are shown. (E) Predicted structures of FN3, FN3-p1 and FN3-p1.M.1–M.3 showing the GA site (pink) and the grafted HBPs (blue).

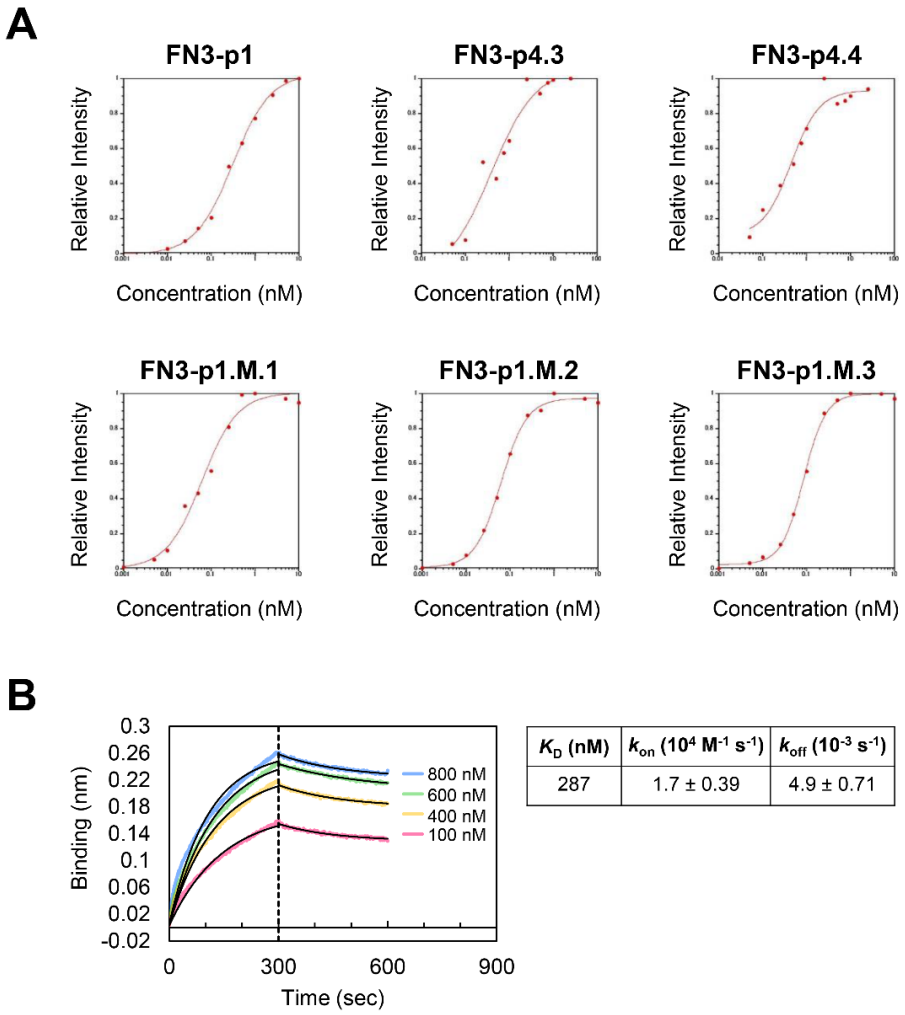

K_D (nM)	k_{on} (10^4 M^{-1} s^{-1})	k_{off} (10^{-3} s^{-1})
287	1.7 ± 0.39	4.9 ± 0.71

Figure 4-3-3-2. Affinity evaluation by ELISA (A) and biolayer interferometry (B). (A) HER2-Fc was immobilized on ELISA plates and exposed to various concentrations of FN3-p1, FN3-p4.3, FN3-p4.4, FN3-p1.M.1, FN3-p1.M.2 or FN3-p1.M.3 proteins with His-tag. Binding was detected with an HRP-conjugated anti-His tag antibody. The results are representative of three experiments. (B) Biotinylated HER2-Fc was immobilized on streptavidin biosensors and exposed to several concentrations of HBP-FLAP. The representative sensorgrams from three experiments (left) and binding kinetics (right) were shown.

Table 4-3-3-1. Dissociation constant of FLAP candidates

F-body or F-body II	K_D (nM)
FN3-p1	280 ± 23
FN3-p4.3	450 ± 74
FN3-p4.4	500 ± 150
FN3-p1.M.1	68 ± 14
FN3-p1.M.2	58 ± 5.0
FN3-p1.M.3	109 ± 28

Table 4-3-3-2. Amino acid sequences of HBPs on FN3-p1

Peptides	Amino acid sequences
p1.1A	ACGCEM
p1.2A	YAGCEM
p1.3A	YCACEM
p1.4A	YCGAEM
p1.5A	YCGCAM
p1.6A	YCGCEA
p1.M.1	YCICCM
p1.M.2	YCAHNM
p1.M.3	YCPVCM

4-3-4. Proteolytic resistance of HBP-FLAP

The protease resistance of p1.M.2 peptide (YCAHNM) was evaluated by treatment with proteinase K, which cleaves peptide bond adjacent to the carboxyl group of the 1st (Y) and 3rd (A) residues (**Fig. 4-3-4-1A**). A C-terminally elongated synthetic p1.M.2 peptide (YCAHNM-GSGSGK) was used for easy detection of peptide-proteolysis by HPLC. As expected, the p1.M.2 peptide in FN3 was resistant to proteinase K treatment for 2 h, whereas the linear p1.M.2 was digested within 10 min (**Figs. 4-3-4-1B** and **4-3-4-2**). The FN3.p1.M.2 hereinafter referred to as HBP-FLAP was then tested the binding specificity and *in vivo* applicability in the next chapter.

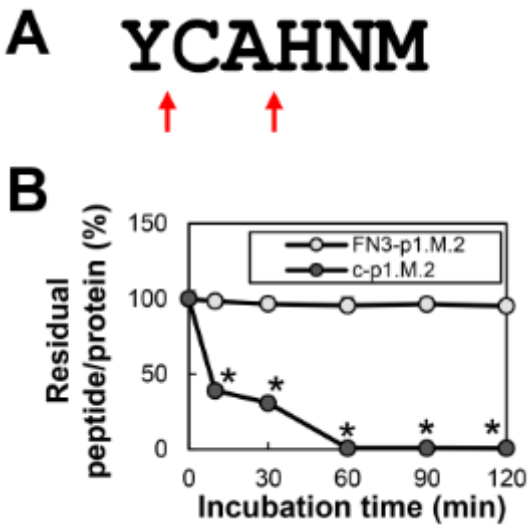

Fig. 4-3-4-1. Proteinase K resistance of the p1.M.2 peptide and FN3-p1.M.2. (A) Cleavage sites of the p1.M.2 peptide by Proteinase K. Peptide bonds adjacent to the carboxyl group of the 1st (Y) and 3rd (A) residues are cleaved (red arrows). (B) Proteinase K resistance of p1.M.2 peptides. FN3-p1.M.2 and the C-terminally elongated p1.M.2 peptide (c-p1.M.2) were analyzed at 10, 30, 60, 90 and 120 min after Proteinase K incubation. Percentage of intact FN3-p1.M.2 and the C-terminally elongated p1.M.2 peptide was calculated by SDS-PAGE and HPLC analysis, respectively. $n = 3$, mean ± SEM, $*p < 0.05$ compared with incubation time at 0 min based on a Student's *t*-test.

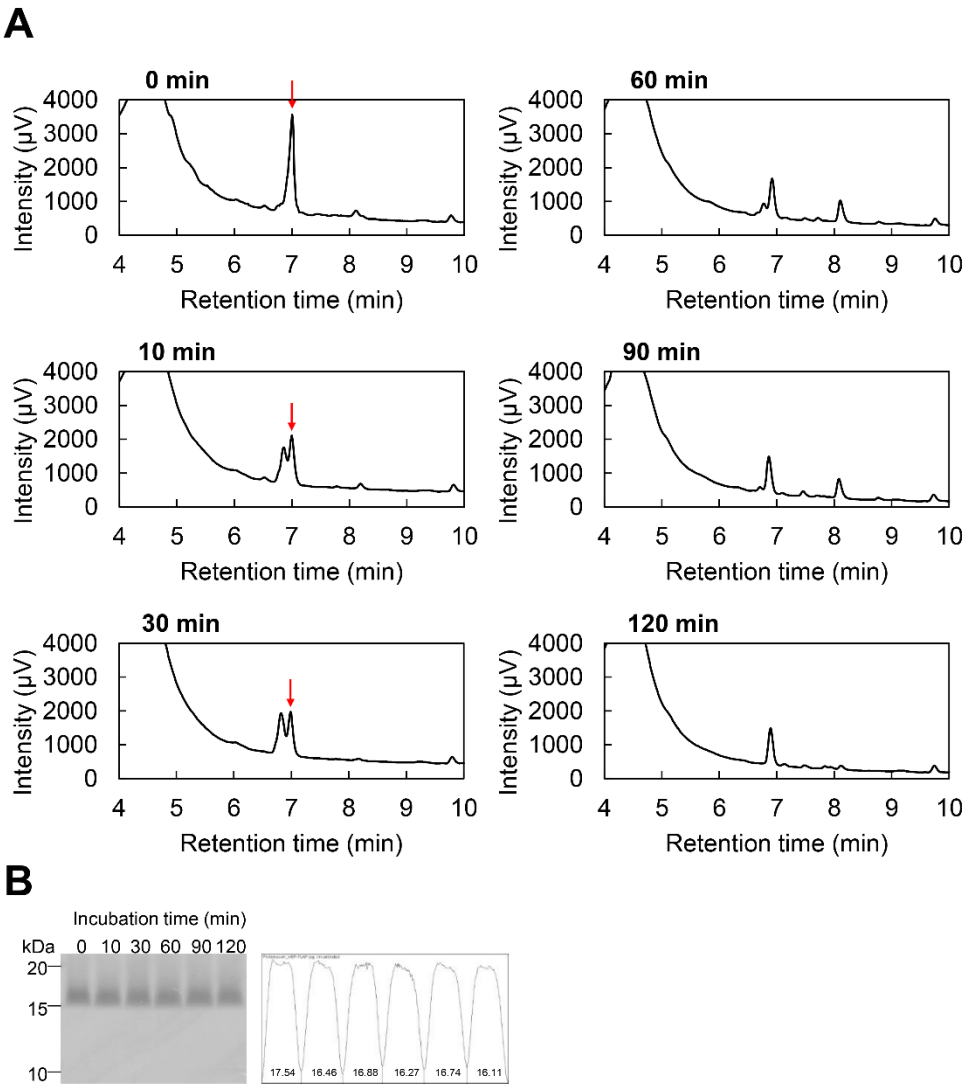

Fig. 4-3-4-2. Proteinase K digestion. (A) HPLC analysis of p1.M.2 peptide digestion by proteinase K. C-terminally elongated peptides appeared at 7 min (red arrow) in retention time. (B) SDS-PAGE analysis (left panel) and a measurement of band intensity (right panel) of FN3-p1.M.2 treated with proteinase K at the indicated times.

4-3-5. Binding specificity of HBP-FLAP

The specificity of HBP-FLAP for HER2-Fc was further confirmed by an ELISA using HER2-Fc- and epidermal growth factor receptor (EGFR)-Fc-coated wells: HBP-FLAP efficiently bound to HER2-Fc but hardly bound to EGFR-Fc-coated wells (**Fig. 4-3-5**). These results showed that the HBP-FLAP has high specificity for HER2.

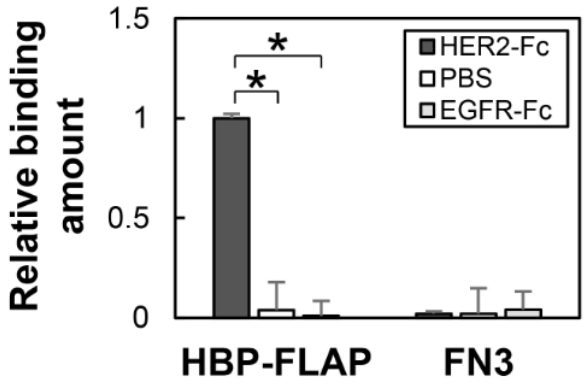

Fig. 4-3-5. Specific binding of HBP-FLAP to HER2. HBP-FLAP binding to HER2-Fc, non-coated well (PBS) or EGFR-Fc were evaluated by ELISA. The mean ± SEM of three independent experiments is shown; *$p < 0.05$.

Discussion

This study demonstrates the creation and evaluation of a HER2-binding small protein called FN3.p1.M.2 or HBP-FLAP that efficiently binds HER2 and increases proteolytic resistance of HBP. FN3-HBPs are created by substituting the HBP hexapeptides with the residues 51-56 of FN3 that was identified as an optimal GA site, in which grafted peptides can be immobilized with average RMSF value less than 1.5 Å (Chapter 2 and 3). In the evaluation of FN3-HBPs (Figs. 4-3-2D and 4-3-3-1A), all grafted hexapeptides were immobilized into the FN3 scaffold and three FN3-HBPs bound to HER2, whereas the other FN3-HBPs may lose critical residues for binding. This result shows that the design method of FLAP is a promising strategy to develop target-binding proteins by grafting target-binding peptides to the GA site of the FN3 scaffold and can contribute to the development of clinically applicable target-binding proteins.

Compared to HBP, HBP-FLAP was more resistant to proteinase K (Fig. 4-3-4-1). The HBP of HBP-FLAP must be exposed on the surface of the molecule because the GA site was selected because it is a solvent exposed loop in the FN3 structure.[14] Therefore, the proteolysis resistance of the HBP in HBP-FLAP is not because of reduced protease access to the target sequence but is likely due to its immobilized structure, which restricts protease activity.

The linear HER2-targeting peptide $(KCCYSL)^2$ and cyclic peptide $(FCGDGFYACYMDV)^4$ reported in other studies showed less serum stability, which might be caused by susceptibility to proteases. These peptides were PEGylated to increase resistance to proteases and the molecular mass, resulting in prolonged blood circulation.[15,16] Another study demonstrated that conjugation of a bicyclic peptide to an albumin-binding peptide increased proteolysis-resistance.[17]

Our study reported a different strategy to improve the proteolysis-resistance of HBP by peptide grafting, which directly immobilized the conformation of the peptide. The property of HBP-FLAP may contribute to the applicability *in vivo*.

References

1. Marqus, S., Pirogova, E. & Piva, T. J. Evaluation of the use of therapeutic peptides for cancer treatment. *J. Biomed. Sci.* **24**, (2017).
2. Karasseva, N. G., Glinsky, V. V., Chen, N. X., Komatireddy, R. & Quinn, T. P. Identification and characterization of peptides that bind human ErbB-2 selected from a bacteriophage display library. *J. Protein Chem.* **21**, 287–296 (2002).
3. Diderich, P. & Heinis, C. Phage selection of bicyclic peptides binding Her2. *Tetrahedron* **70**, 7733–7739 (2014).
4. Park, B. W. *et al.* Rationally designed anti-HER2/neu peptide mimetic disables p185(HER2/neu) tyrosine kinases in vitro and in vivo. *Nat. Biotechnol.* **18**, 194–198 (2000).
5. Honarvar, H. *et al.* Evaluation of HER2-specific peptide ligand for its employment as radiolabeled imaging probe. *Sci. Rep.* **8**, 2998 (2018).
6. Yang, X. *et al.* Peptide probes derived from pertuzumab by molecular dynamics modeling for HER2 positive tumor imaging. *PLoS Comput. Biol.* **13**, e1005441 (2017).
7. Lipovšek, D. Adnectins: engineered target-binding protein therapeutics. *Protein Eng. Des. Sel.* **24**, 3–9 (2011).
8. Hantschel, O., Biancalana, M. & Koide, S. Monobodies as enabling tools for structural and mechanistic biology. *Curr. Opin. Struct. Biol.* **60**, 167–174 (2020).
9. Bloom, L. & Calabro, V. FN3: a new protein scaffold reaches the clinic. *Drug Discov. Today* **14**, 949–955 (2009).
10. Schiff, D. *et al.* Phase 2 study of CT-322, a targeted biologic inhibitor of

VEGFR-2 based on a domain of human fibronectin, in recurrent glioblastoma. *Invest. New Drugs* **33**, 247–253 (2015).

11. Hatanaka, T. *et al.* Human IgA-binding peptides selected from random peptide libraries: Affinity maturation and application in IGA purification. *J. Biol. Chem.* **287**, 43126–43136 (2012).
12. Case, D. A. *et al. Amber 2017*. *University of California, San Francisco* (2017). doi:citeulike-article-id:2734527
13. Kadonosono, T. *et al.* A fluorescent protein scaffold for presenting structurally constrained peptides provides an effective screening system to identify high affinity target-binding peptides. *PLoS One* **9**, e103397 (2014).
14. Kadonosono, T. *et al.* Design Strategy to Create Antibody Mimetics Harbouring Immobilised Complementarity Determining Region Peptides for Practical Use. *Sci. Rep.* **10**, 891 (2020).
15. Guan, S. S. *et al.* Polyethylene glycol-conjugated HER2-targeted peptides as a nuclear imaging probe for HER2-overexpressed gastric cancer detection in vivo. *J. Transl. Med.* **16**, 168 (2018).
16. Bandekar, A. *et al.* Masking and triggered unmasking of targeting ligands on liposomal chemotherapy selectively suppress tumor growth in vivo. *Mol. Pharm.* **10**, 152–160 (2013).
17. Pollaro, L. *et al.* Bicyclic peptides conjugated to an albumin-binding tag diffuse efficiently into solid tumors. *Mol. Cancer Ther.* **14**, 151–161 (2015).

Chapter 5

Specific binding of FLAPs to HER2-overexpressing cells *in vitro* and *in vivo*

Abstract

One common use of mAbs other than molecular targeting drugs is diagnostic probes, especially for immunostaining, immunohistochemistry (IHC) or *in vivo* imaging. Alternatives to antibody, such as small target-binding proteins, are attractive option because their size can facilitate tissue penetration and reduce analytical costs. In this chapter, I evaluated the applicability of FLAPs for targeting HER2-overexpressing cells *in vitro* and *in vivo*. Four FLAPs identified in Chapter 3 and 4, AbP-FLAP 1, 2, 3 and HBP-FLAP, bound only to high HER2-expressing cells and not to control cells, indicating that FLAPs could be developed as mAb replacement for IHC. In addition, HBP-FLAP clearly delineated HER2-expressing tumors with a half-life of 6 h after intravenous injection into tumor-bearing mice. FN3-based FLAP is an excellent platform for developing target-binding small proteins for clinical applications.

5-1. Introduction

5-1-1. Immunohistochemistry

IHC is one of the common techniques of immunostaining, an mAb-based method to detect specific proteins or antigens in samples.[1] The mAb-based staining methods involve in several techniques such as flow cytometry, western blotting, ELISA and immuno-electron microscopy. To date, immunostaining is widely used in histology, cell biology and molecular biology. IHC is typically used for clinical diagnostics of cancer and medical research laboratories. The detection strategy of IHC utilize mAbs are classified as primary and secondary reagents. Basically, the unlabeled primary mAbs are raised against an antigen of interest, while secondary mAbs usually conjugated with biotin, enzyme or fluorescent dye are raised against immunoglobulins of the primary mAb species.[2]

In order to overcome some limitations of Abs as mentioned before, numerous Ab fragments and Ab mimetics have been extensively developed for IHC applications such as V_{HH} antibody (or nanobody),[3] affibody,[4] or affimers.[5]

In this chapter, according to the properties of FN3-based scaffold, I also aim to validate the utility of AbP-FLAPs and HBP-FLAP for detection of HER2-overexpressing cancer cells.

5-1-2. *In vivo* stability of small therapeutic proteins or peptides

Although the tumor-binding peptides are a promising alternative to mAbs, their clinical application is limited to use as diagnosis probes because short peptides are very sensitive to protease activity in circulation and tissues, resulting in reduced binding to targets. Several strategies have been developed to increase proteolysis-resistance of peptides *in vivo*, including conjugation of peptides to macromolecules,

including polyethylene glycol (PEG), the Fc domain or serum albumin.[6] Cyclization of peptides or grafting of peptide into cyclic peptide are also simple strategies to increase resistance to proteases.[7,8] Recent study found that the affinity and proteolysis-resistance of peptides was greatly improved after their structure was immobilized by grafting into a particular site of a protein scaffold.[9] Based on this finding, a computational design strategy for developing antibody mimetics named FLAP are reported on Chapter 2–4.

Chapter 4 showed that protease resistance of HBP was increased in HBP-FLAP. In this chapter, the HBP-FLAP was prepared as imaging probe and the *in vivo* retention was examined in N87 tumor-bearing mice.

5-2. Materials and Methods

5-2-1. Cell immunostaining

The human cervical cancer cell line HeLa and human gastric cancer cell line N87 or human breast cancer cells expressing firefly luciferase SK-BR-3/Luc were obtained from the RIKEN Bio-Resource Center (Tsukuba, Japan) or JCRB Cell Bank (Osaka, Japan), respectively and maintained at 37 °C in 5% FBS-DMEM (Nacalai Tesque, Kyoto, Japan) supplemented with penicillin (100 U/ml) and streptomycin (100 μg/ml) (Nacalai Tesque). The cells (1.0×10^4 cells/well) were seeded on a slide chamber plate, cultured for 16 h and fixed by treatment with a 4% paraformaldehyde solution (Nacalai Tesque) for 10 min at 25 °C. The cells were blocked with 1% BSA/PBS for 1 h at 25 °C. After the addition of 50 nM purified His-tagged AbP-FLAPs or 100 nM purified His-tagged HBP-FLAP or 5 nM trastuzumab in 1% BSA/PBS to the chamber, the cells were incubated for 16 h at 4 °C. Thousand-fold diluted Alexa Fluor 488-conjugated mouse anti-His tag secondary antibody (Medical & Biological Laboratories, Aichi, Japan) or Alexa Fluor 488-conjugated mouse anti-human IgG Fc secondary antibody in 1% BSA/PBS were used to fluorescently label the His-tagged FLAPs or trastuzumab, respectively. After washing three times with PBS, the stained cells were mounted with Fluoromount (Diagnostic ByoSystems, CA, USA) containing 1/1000 Hoechst 33342 (Nacalai Tesque). All photos were taken using a BZ-X700 microscope (Keyence, Osaka, Japan) with the filters of BZ-X filter GFP, OP-87763 (Ex: 470/40 nm, Em: 525/50 nm) and BZ-X filter DAPI, OP-87762 (Ex: 360/40 nm, Em: 460/50 nm).

5-2-2. Flow cytometry

Single cell suspensions of HeLa, SK-BR-3 and N87 cells (1.0×10^5 cells/100 μL) were incubated in PBS containing 1000 times-diluted Alexa Fluor 488 anti-human HER2 antibody (clone 24D2; BioLegend, San Diego, CA, USA) on ice in the dark for 30 min. Cells without immunostaining were used as a negative control. Flow cytometry was performed by a flow cytometer ec800 (Sony Biotechnology, San Jose, CA, USA).

5-2-3. Plasmid construction and protein purification

The recombinant DNA experiment was carried out according to the necessary regulations based on the Tokyo Institute of Technology recombinant DNA experimental safety management regulations defined by the Tokyo Institute of Technology recombinant DNA experimental safety management committee. The cDNA encoding fusion protein composed of His-tag, GGGS linker and FN3 (H-FN3) was inserted into the multi-cloning site of pGEX-6P-3 plasmid (GE Healthcare, Little Chalfont, UK).[10] The cDNA encoding C-terminally CTag (GMAQIEVNCSNE)[11]-fused His-tagged FLAP (H-FLAP-C) or C-terminally CTag-fused H-FN3 (H-FN3-C) were constructed by site-directed mutagenesis of H-FN3 cDNA as the template. The plasmid vectors expressing H-FN3-C and H-FLAP-C were transformed into *E. coli* BL21 (DE3) pLysS cells (Promega, Fitchburg, WI, USA). These proteins were expressed in the bacteria as GST fused proteins. GST-fused H-FN3-C and H-FLAP-C were purified from the supernatants of bacterial extracts using glutathione agarose (Sigma-Aldrich, MO, USA). After protease-cleavage of GST by PreScission Protease (GE Healthcare), monomeric proteins were purified using HisTrap HP columns (GE Healthcare), according to

the manufacturer's instructions.

5-2-4. Preparation of HBP-FLAP and FN3 probes

HBP-FLAP-IR800 and FN3-IR800 monomer probes were prepared by covalent conjugation of a fluorescent dye IRDye 800CW-maleimide (LI-COR Biosciences, Lincoln, NE, USA) to a cysteine residue at the C-terminus of the CTag of H-FLAP-C. Twenty-five nmol of unlabeled H-FLAP-C or H-FN3-C was reacted with 50 nmol of IRDye 800CW-maleimide in PBS for 2 h at room temperature. PD-10 desalting columns (GE healthcare) were used to purify the reactants.

5-2-5. Mice and *in vivo* fluorescent imaging

All animal experiments were performed with the approval of the Animal Ethics Committees of Tokyo Institute of Technology (No. 2017004) and in accordance with the Ethical Guidelines for Animal Experimentation of Tokyo Institute of Technology. Male BALB/c nude mice were purchased from Oriental Yeast Co., Ltd. (Tokyo, Japan). All mice used were 6–9 weeks of age. For the subcutaneous xenograft model, N87 cells suspended in PBS (1.0×10^6 cells/20 μL) were mixed with an equal volume of Geltrex (Life Technologies) and injected into the forefoot of mice. Mice with subcutaneous tumors of 10–15 mm in diameter were used for experiments. To acquire fluorescence images, 300 pmol in 100 μL PBS of HBP-FLAP-IR800 or FN3-IR800 was intravenously injected into mice with subcutaneous tumors in the forefoot. The following conditions were used for image acquisition: excitation filter = 710 ± 15 nm; emission filter = 800 ± 10 nm; and exposure time = 1 s. The minimum and maximum photons/s/cm^2/sr of each image are indicated in each figure by a yellow-red bar scale.

5-2-6. Statistical analysis

Data in this study are expressed as means ± SEM. Differences are analyzed with a two-sided Student's *t*-test; *p* values of <0.05 were considered as statistically significant.

5-3. Results

5-3-1. FLAP potentially detect HER2-overexpressing cancer cells

The binding specificity of three AbP-FLAP candidates and HBP-FLAP, was evaluated using cell lines expressing different levels of HER2. HeLa cells (no HER2 expression), SK-BR-3 cells (HER2 expression) or N87 cells (HER2 expression) were incubated with four FLAPs, followed by staining with a fluorescently labelled anti-His-tag antibody that binds to the His-tag at the N-terminus of FN3. A strong fluorescence was observed in SK-BR-3 and N87 cells, but not HeLa cells (**Fig. 5-3-1**). These results indicate that the FLAPs specifically detect HER2-overexpressing cells.

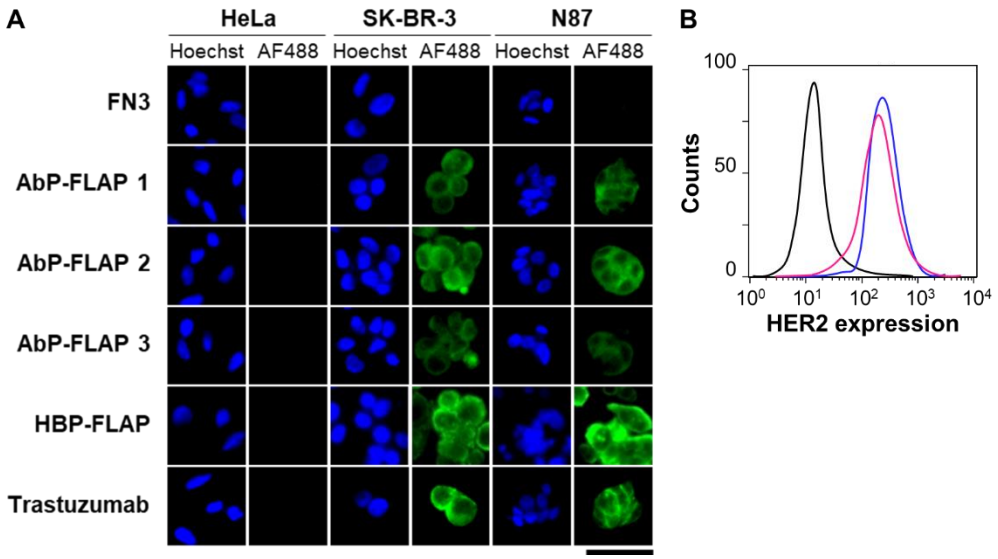

Fig. 5-3-1. Detection of HER2-overexpressing cancer cell lines by FLAPs. (A) Immunostaining of HeLa, SK-BR-3/Luc or N87 cells with His-tagged FLAPs or trastuzumab (green) and Hoechst (blue). Scale bar = 50 μm. (B) Flow cytometry analysis of HER2 expression on the cell surface of HeLa (black line), SK-BR-3 (blue line) and N87 (magenta line) cells. Histograms are representative of two experiment.

5-3-2. *In vivo* fluorescent imaging of a HER2-expressing tumor by HBP-FLAP

To assess the applicability of HBP-FLAP as a probe for targeting a HER2-expressing tumor *in vivo*, the HBP-FLAP and FN3 scaffold were labeled with a near-infrared fluorescent dye IR800CW (HBP-FLAP-IR800 and FN3-IR800; MW = 10 kDa) (**Figs. 4-3-1D** and **5-3-2A**). *In vivo* imaging was performed at various post-injection (p.i.) times to monitor HBP-FLAP-IR800 and FN3-IR800 probes in N87 tumor-bearing nude mice. Although similar fluorescent intensities were observed in tumors at 0.5 h p.i. of the probes, higher fluorescent signals were detected at longer periods in tumors from mice injected with HBP-FLAP-IR800 (**Fig. 5-3-2B** and **C**). HBP-FLAP-IR800 specifically accumulated at HER2-expressing tumors with higher T/B ratios when compared with that of FN3-IR800 (**Fig. 5-3-2D**). As expected from the molecular weight of the probes, both probes were mainly excreted through the urinary system (**Fig. 5-3-2B**). These results suggested that binding to HER2 retained HBP-FLAP for longer periods in tumors and that the HBP-FLAP design is a promising strategy for developing clinically applicable small proteins using target-binding peptides.

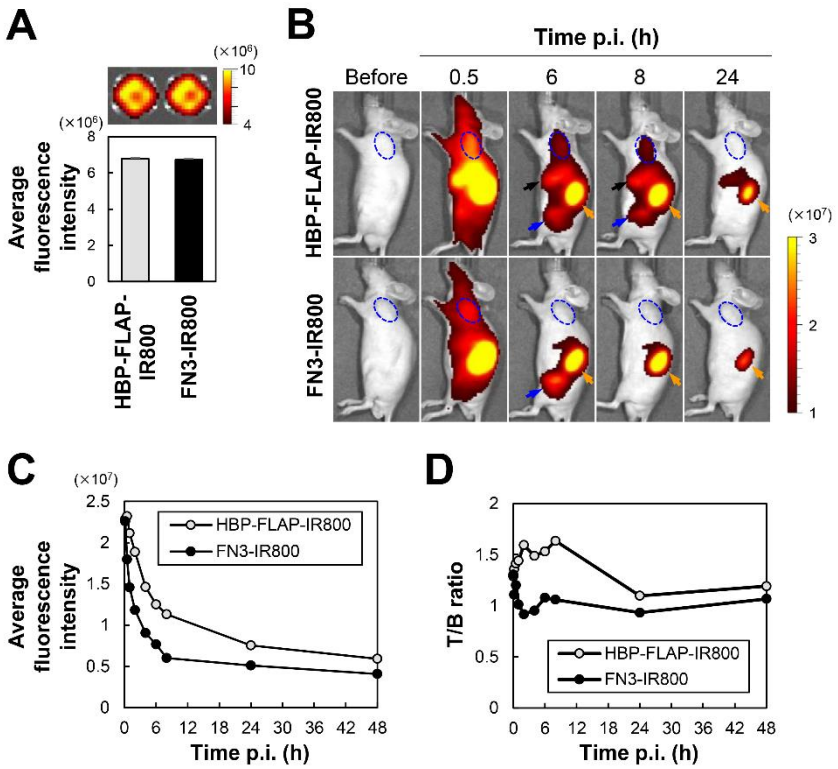

Figure 5-3-2. *In vivo* fluorescence imaging of a HER2-expressing tumor. (A) Average fluorescent intensity (photons/s/cm²/sr) of HBP-FLAP-IR800 and FN3-IR800 probe before i.v. injection; n = 3, mean ± SEM. (B) Representative *in vivo* images of N87 tumor-bearing mice at the indicated times of p.i. of the probes shown in (A). A dashed blue circle indicates the tumor, a black arrow indicates the liver, an orange arrow indicates the kidney and the blue arrow indicates the bladder. (C) Average fluorescent intensity (photons/s/cm²/sr) of HBP-FLAP-IR800 and FN3-IR800 probes in tumors. (D) The ratio of tumor (fluorescence intensity of tumors) versus background (fluorescence intensity of muscles) (T/B ratio) of HBP-FLAP-IR800 and FN3-IR800 probes at the indicated times of p.i.

Discussion

In this chapter, FLAPs represented specific binding to HER2-overexpressing cancer cells (SK-BR-3 and N87 cell lines) and showed applicability for targeting HER2-expressing tumors *in vivo* (Figs. 5-3-1 and 5-3-2). Although target-binding peptides/proteins selected by *in vitro* screening may bind to off-targets *in vivo*, HBP-FLAP likely binds to HER2 specifically because no detectable signal was observed in parts of the body other than HER2-expressing tumors and excretion organs (Fig. 5-3-2B).

The FLAP design might be a preferable strategy for developing clinically applicable proteolysis-resistant molecules from target-binding peptides when compared with cyclization or grafting into cyclic peptide approaches, because many proteins with a variety of molecular sizes and charges can be used as scaffolds for developing FLAPs. Therefore, the *in vivo* retention time of FLAPs can be optimized by using the appropriate scaffolds. In comparison to other strategies such as PEGylation, Fc-fusion and albumin-fusion, in which either the C- or N-terminus of the target-binding peptides is exposed, the FLAP design can mask both termini by covalent conjugation with the scaffold, suggesting that peptides in FLAP also show higher proteolysis-resistance to exo-proteases in the body when compared with that of peptides with other modifications.

The application of HBP-FLAP as a diagnostic probe (*in vitro* immunostaining and *in vivo* imaging) was shown in this study. To address the applicability of HBP-FLAP for tumor treatment, I need to further evaluate inhibition of HER2-signaling, cancer cell proliferation and tumor growth. Theragnostic probes by radioisotope- and near-infrared dye-conjugations are also possible applications of FLAPs.

References

1. O'Hurley, G. *et al.* Garbage in, garbage out: A critical evaluation of strategies used for validation of immunohistochemical biomarkers. *Mol. Oncol.* **8**, 783–798 (2014).
2. Ivell, R., Teerds, K. & Hoffman, G. E. Proper application of antibodies for immunohistochemical detection: Antibody crimes and how to prevent them. *Endocrinology* **155**, 676–687 (2014).
3. Perruchini, C. *et al.* Llama VHH antibody fragments against GFAP: Better diffusion in fixed tissues than classical monoclonal antibodies. *Acta Neuropathol.* **118**, 685–695 (2009).
4. Lyakhov, I. *et al.* HER2- and EGFR-specific affiprobes: Novel recombinant optical probes for cell imaging. *ChemBioChem* **11**, 345–350 (2010).
5. Tiede, C. *et al.* Affimer proteins are versatile and renewable affinity reagents. *Elife* **6**, 1–35 (2017).
6. AlQahtani, A. D., O'Connor, D., Domling, A. & Goda, S. K. Strategies for the production of long-acting therapeutics and efficient drug delivery for cancer treatment. *Biomed. Pharmacother.* **113**, 108750 (2019).
7. Conibear, A. C. *et al.* Approaches to the stabilization of bioactive epitopes by grafting and peptide cyclization. *Biopolymers* **106**, 89–100 (2016).
8. Wang, C. K. *et al.* Molecular grafting onto a stable framework yields novel cyclic peptides for the treatment of multiple sclerosis. *ACS Chem. Biol.* **9**, 156–163 (2014).
9. Kadonosono, T. *et al.* A fluorescent protein scaffold for presenting structurally constrained peptides provides an effective screening system to identify high affinity target-binding peptides. *PLoS One* **9**, e103397 (2014).

10. Sambrook, J., Fritsch, E.F., and Maniatis, T. Molecular Cloning: A Laboratory Manual. Cold Spring Harbor Laboratory Press, New York. *Cold Spring Harb. Lab. Press* **61**, 17–18 (1989).

11. Dong, J., Kojima, T., Ohashi, H. & Ueda, H. Optimal fusion of antibody binding domains resulted in higher affinity and wider specificity. *J. Biosci. Bioeng.* **120**, 504–509 (2015).

Chapter 6

Conclusion and prospect

Small proteins that chemically synthesizable and specifically bind to cancer cell markers are promising alternatives to Ab mimetics. These small proteins overcome some limitations of Ab such as high molecular weight, limited tissue penetration, and high production cost. Therefore, various types of Ab mimetics have been extensively developed. Based on our recent study, a structural immobilization of the target-binding peptides by grafting to a particular site of a fluorescent protein scaffold increases their binding affinity. In this study, I aimed to develop fluctuation-regulated affinity proteins (FLAPs) consisting of a small immunocompatible scaffold protein and a hexapeptide that specifically binds to HER2, a breast cancer marker. The small scaffold proteins and GA sites were first selected (Chapter 2). FLAP candidates were designed and created using two strategies in parallel (Chapter 3 and 4), and evaluated for HER2-binding activities to identify FLAPs that specifically bind to HER2-expressing cancer cells (Chapter 3–5). I also examined the *in vivo* applicability of a FLAP as an imaging probe for HER2-expressing tumors (Chapter 5).

Chapter 2 explains the computational selection of small protein scaffolds and identification of GA sites. To develop FLAPs, I initially selected 13 non-Ig human protein scaffold candidates that had sizes amenable to chemical synthesis and a low number of disulfide bonds, and then identified six suitable proteins using the validation method. The appropriate GA sites in the scaffold candidates were evaluated by a unique method using MD simulation. Finally, 13 GA sites in 6 scaffolds were selected for FLAP construction.

Chapter 3 describes the design and evaluation of FLAPs in which HER2-binding sequences were extracted from anti-HER2-mAbs. Five AbPs were extracted by binding energy calculations of CDR peptides of clinically used anti-

HER2 mAbs, trastuzumab and pertuzumab, and grafted into the 13 selected GA sites, resulting in 65 FLAP combinations. Four out of 65 FLAP candidates showed strong binding to HER2 with K_D of 24–65 nM in ELISA and 270–350 nM in biolayer interferometry. Three out of four candidates had FN3 scaffold and bound to the same epitope as trastuzumab, hereinafter regard these candidates as AbP-FLAPs.

Chapter 4 describes the design and evaluation of FLAPs in which HBPs were selected by screening a peptide library. The HBPs were first isolated from a phage-displayed peptide library and grafted into GA sites of FN3 to create FN3-HBPs. Binding affinity of the FN3-HBPs was then improved by affinity maturation. The affinity-matured FN3-HBP, hereinafter referred to as HBP-FLAP, showed clinically relevant binding affinity (K_D = 58 nM in ELISA and 287 nM in biolayer interferometry). In addition, proteolytic resistance of HBP was improved in HBP-FLAP. This property of HBP-FLAP may contribute to the long retention time *in vivo*.

Chapter 5 describes the applicability of FLAPs as diagnostic probes.For *in vitro* immunostaining, three AbP-FLAPs and one HBP-FLAP bound to high HER2-expressing cells (SK-BR-3 and N87 cells) but hardly to control cells (HeLa cells with low or no HER2 expression). This result suggests that FLAPs might be able to use for other Ab-based applications. For *in vivo* imaging, HBP-FLAP was able to delineate HER2-overexpressing tumors with a half-life of 6 h after intravenous injection to the tumor-bearing mice. These results indicate that FLAPs specifically bind to the target and are applicable to both *in vitro* and *in vivo*.

The final goal of this research is development of HER2-targeting small proteins by immobilization of binding peptides into small protein scaffolds. In this study, I

have demonstrated a successful creation of FLAPs by grafting structurally immobilized AbPs or HBPs into non-Ig scaffolds. A strategy for creation of AbP-FLAPs is applicable for other mAbs and other functional proteins. Moreover, a strategy to create HBP-FLAP is not only found new HBP, but also increase proteolytic resistance of the HBP. Although the binding affinity of FLAPs is moderate, this may have the advantage of reducing toxicity due to on-target off-tumor binding. Since FLAPs are generated from small protein scaffolds of the size less than 120 amino acid, this chemical synthesizable property might be additional benefit of production. Due to the specific binding property, FLAPs would be able to use for several applications such as diagnosis probe or use as a small protein drug.

Overall, I hope that the efficient and practical method of FLAP development can be applied to many therapeutic targets, not only cancer but also other diseases where antibodies and recombinant proteins are currently used. Therefore, this study may open new avenues for developing novel technology platforms in protein engineering and biopharmaceutical design.

Achievements

Publications

Yimchuen, W., Kadonosono, T., Ota, Y., Sato, S., Kitazawa, M., Shiozawa, T., Kuchimaru, T., Taki, M., Ito, Y., Nakamura, H., and Kizaka-Kondoh, S. Strategic design to create HER2-targeting proteins with target-binding peptides immobilized on a fibronectin type III domain scaffold. *RSC Adv.* **10**, 15154-15162. (2020). doi: 10.1039/d0ra00427h.

Kadonosono, T., Yimchuen, W., Ota, Y., See, K., Furuta, T., Shiozawa, T., Kitazawa, M., Goto, Y., Patil, A., Kuchimaru, T., and Kizaka-Kondoh, S. Design Strategy to Create Antibody Mimetics Harbouring Immobilised Complementarity Determining Region Peptides for Practical Use. *Sci Rep*. **10**, 891. (2020). doi: 10.1038/s41598-020-57713-4.

Conference Presentation

<Oral presentation>

Yimchuen, W., Kadonosono, T., Furuta, T., Shiozawa, T., Kitazawa, M., Kuchimaru, T., Sakurai, M., and Kizaka-Kondoh, S. Evaluation of immunoglobulin-based antibody mimetics with a constrained target-binding peptide. The 53rd Japanese Peptide Symposium, October 26–28, 2016 (Kyoto, Japan).

<Poster presentation>

Yimchuen, W., Kadonosono, T., Sato, S., Nomoto, T., See, K., Kuchimaru, T., Nakamura, H., Nishiyama, N., and Kizaka-Kondoh, S. Development of photoimmunotherapy probe using a small antibody mimetic with structurally constrained anti-HER2 CDR peptides. The 26th American Peptide Symposium, June 22–27, 2019 (California, U.S.).

Yimchuen, W., Kadonosono, T., Sato, S., See, K., Kuchimaru, T., Nakamura, H., and Kizaka-Kondoh, S. Creation of a small antibody mimetic immunoprobe with structurally constrained anti-HER2 CDR peptides. The 10th International Peptide Symposium, December 3–7, 2018 (Kyoto, Japan).

Yimchuen, W., Kadonosono, T., Sato, S., Nakamura, H., See, K., Kuchimaru, T., and Kizaka-Kondoh, S. Development of small antibody mimetics with high-affinity and specificity for imaging and targeting HER2-positive tumors using structurally constrained CDR peptides. The 41st Annual Meeting of the Molecular Biology Society of Japan, November 28–30, 2018 (Kanagawa, Japan).

Yimchuen, W., Kadonosono, T., See, K., Kuchimaru, T., and Kizaka-Kondoh, S. Functional analysis of high-affinity antibody mimetics with structurally constrained CDR

peptides for tumor imaging. In vivo イメージングフォーラム 2018 [第 13 回 IVIS ユーザー会], October 19, 2018 (Tokyo, Japan).

Yimchuen, W., Kadonosono, T., See, K., Kuchimaru, T., and Kizaka-Kondoh, S. Functional analysis of high-affinity antibody mimetics with structurally constrained CDR peptides for tumor imaging. The 77th Annual Meeting of the Japanese Cancer Association, September 27–29, 2018 (Osaka, Japan).

Yimchuen, W., Kadonosono, T., See, K., Kuchimaru, T., and Kizaka-Kondoh, S. Development of high-affinity tumor imaging probes with structurally constrained CDR peptides. The 13rd Japanese Society for Molecular Imaging, May 31–June 1, 2018 (Tokyo, Japan).

Yimchuen, W., Kadonosono, T., See, K., Kuchimaru, T., and Kizaka-Kondoh, S. Development of anti-HER2 antibody mimetics with structurally constrained CDR peptides. The 54th Japanese Peptide Symposium, November 20–22, 2017 (Osaka, Japan).

Yimchuen, W., Kadonosono, T., See, K., Kuchimaru, T., and Kizaka-Kondoh, S. Development of high-affinity tumor imaging probes based on constrained target-binding peptides. The 12th Japanese Society for Molecular Imaging, May 25–26, 2017 (Kanagawa, Japan).

Yimchuen, W., Kadonosono, T., Furuta, T., Shiozawa, T., Kitazawa, M., Kuchimaru, T., Sakurai, M., and Kizaka-Kondoh S. Development of IgG-based antibody mimetics with a constrained target-binding peptide. The 39th Annual Meeting of the Molecular Biology Society of Japan, November 30–December 2, 2016 (Kanagawa, Japan).

Yimchuen, W., Kadonosono, T., Shiozawa, T., Kitazawa, M., Kuchimaru, T., and Kizaka-Kondoh, S. Development of IgG-based small antibody mimetics containing a constrained target-binding peptide. The 75th Annual Meeting of the Japanese Cancer Association, October 6–8, 2016 (Kanagawa, Japan).

Acknowledgement

Foremost, I owe my deepest appreciation to my supervisors, Prof. Shinae Kizaka-Kondoh and Asst. Prof. Tetsuya Kadonosono of the department of Life Science and Technology, School of Life Science and Technology, Tokyo Institute of Technology for their continuous patience, motivation and immense knowledge. Their guidance helped me all the time from the learning process to writing and edition of this thesis. Their enthusiasm and research attitudes have motivated me to keep moving up in academic learning and research.

I would also like to acknowledge the experts who were involved in this research, Asst. Prof. Takahiro Kuchimaru, for their constructive comments, suggestions, and critiquing.

I would like to thank Assoc. Prof. Masumi Taki, The University of Electro-Communications and Assoc. Prof. Yuji Ito, Kagoshima University for kindly providing T7 phage libraries, Prof. Hiroyuki Nakamura and Asst. Prof. Shinichi Sato, Tokyo Institute of Technology for technical support of HPLC analysis. Prof. Hiroshi Ueda, Tokyo Institute of Technology for the support of biolayer interferometry.

I appreciate the mice that I used for this study and express my condolences from the bottom of my heart. I would like to thank the Open Research Facilities for Life Science and Technology, Tokyo Institute of Technology for sequencing analysis.

My sincere thanks also go to all Kondoh lab stuffs and members, who have helped with the project and supported me in many ways.

Finally, I would like to thank my parents and friends for providing me with unfailing support and continuous encouragement throughout my years of study and through the process of researching and writing this thesis. This accomplishment would not have been possible without them. Thank you.

Wanaporn Yimchuen